scientific reports

OPEN

Multicolor tunable emission through energy transfer in Dy³⁺/Ho³⁺ co-doped CaTiO₃ phosphors with high thermal stability for solid state lighting applications

Priti Singh[1], Hirdyesh Mishra[2] & Shyam Bahadur Rai[1✉]

The exploration of multicolor emitting phosphors with single phase is extremely important for n-UV chip excited LED/WLED's and multicolor display devices. In this paper, Dy³⁺, Ho³⁺ singly doped and Dy³⁺/Ho³⁺ co-doped CaTiO₃ phosphor materials have been synthesized by solid state reaction method at 1473 K. The synthesized materials were characterized by XRD, FE-SEM, EDX, FTIR, PL and lifetime measurements. The PL emission spectra of Dy³⁺ doped CaTiO₃ phosphors give intense blue and yellow emissions under UV excitation, while the PL emission spectra of Ho³⁺ doped CaTiO₃ phosphor show intense green emission under UV/blue excitations. Further, to get the multicolor emission including white light, Dy³⁺ and Ho³⁺ were co-doped simultaneously in CaTiO₃ host. It is found that alongwith colored and white light emissions, it also shows energy transfer from Dy³⁺ to Ho³⁺ with 367 nm and from Ho³⁺ to Dy³⁺ under 362 nm excitations. The energy transfer efficiency is found to be 67.76% and 69.39% for CaTiO₃:4Dy³⁺/3Ho³⁺ and CaTiO₃:3Ho³⁺/5Dy³⁺ phosphors, respectively. The CIE color coordinates, CCT and color purity of the phosphors have been calculated, which show color tunability from whitish to deep green via greenish yellow color. The lifetime of $^4F_{9/2}$ level of Dy³⁺ ion and $^5S_2$ level of Ho³⁺ ion is decreased in presence of Ho³⁺ and Dy³⁺ ions, respectively. This is due to energy transfer from Dy³⁺ to Ho³⁺ ions and vice versa. A temperature dependent photoluminescence studied of CaTiO₃:4Dy³⁺/2Ho³⁺ phosphor show a high thermal stability (82% at 423 K of initial temperature 303 K) in the temperature range 303–483 K with activation energy 0.17 eV. The PLQY are 30%, 33% and 35% for CaTiO₃:4Dy³⁺, CaTiO₃:4Dy³⁺/2Ho³⁺ and CaTiO₃:3Ho³⁺ phosphors, respectively. Hence, Dy³⁺, Ho³⁺ singly doped and Dy³⁺/Ho³⁺ co-doped CaTiO₃ phosphor materials can be used in the field of single matrix perovskite color tunable phosphors which may be used in multicolor display devices, n-UV chip excited LED/WLED's and photodynamic therapy for the cancer treatment.

Lanthanide ions doped phosphor materials produce multicolor tunable emissions under UV, visible or NIR excitations[1–3], which have various applications in multicolor display devices, plasma displays panels (PDP) and light emitting diodes (LED) for solid-state lighting devices[4–6]. Lanthanides are also used in several other areas such as induced optical heating, optical thermometry, bio-imaging, lasers, solar cells and in photodynamic therapy to destroy cancer cells etc[7–11].

The color tunable emission is very interesting property of lanthanide doped/co-doped phosphors. It can be observed by several ways, viz. by varying the concentration of dopants for same excitation wavelength or fixed dopants concentration and varying the excitation wavelength or through energy transfer from sensitizer to activator[12–14]. Chen et al. prepared Sm³⁺ doped $Ca_2NaZn_2V_3O_{12}$ phosphor by solid state reaction method and found the color tunabillity by tuning the Sm³⁺ ion concentration under 365 nm excitation[15]. Lohia et al. reported Eu³⁺ doped $BaZnO_2$ phosphor and studied their photoluminescence emission under different excitation wavelengths (275, 370, 395 & 467 nm) in which the color was found to tune from whitish to red via orange one[16]. The multicolor tunable emission has been seen by many researchers via energy transfer from sensitizer

---

[1]Laser and Spectroscopy Laboratory, Department of Physics, Institute of Science, Banaras Hindu University, Varanasi 221005, India. [2]Physics Section, Mahila Maha Vidhyalaya, Department of Physics, Banaras Hindu University, Varanasi 221005, India. ✉email: sbrai49@yahoo.co.in

1

to activator[17,18]. Förster's and Dexter's theories help to understand the energy transfer process from sensitizer (donor) to activator (acceptor) ions in organic and inorganic materials[19,20]. Qu et al. studied the color tunability in Tb[3+] and Eu^{3+} co-doped $Ca_2YZr_2Al_3O_{12}$ phosphor via energy transfer from Tb[3+] to Eu^{3+} ion[20]. They found that the color changes from green to yellow and then red by varying the concentration of Eu^{3+} ion. Li et al. have reported the color tunability from greenish yellow to red in $KBaY(MoO_4)_3$:Dy[3+],Eu^{3+} phosphor through energy transfer from Dy[3+] to Eu^{3+} ion[21]. Dwivedi et al. observed the multicolor tunable emission through energy transfer in Ho[3+], Eu^{3+} co-doped $Ca_{0.05}Y_{1.93-x}O_2$ nanophosphors[4]. Recently, Rai et al. have also observed color tunability from green to red via orange in $LaVO_4$:Tb[3+]:Eu^{3+} phosphors on varying the concentration of Eu^{3+} ion[22].

Among the lanthanide ions, Dy[3+] and Ho[3+] ions emit effective blue, yellow and green emissions, respectively in almost all hosts[3,6]. The emission from Dy[3+] and Ho[3+] ions individually under UV and blue excitations have been studied by several researchers in different hosts[23–27]. The blue emission of Dy[3+] and green emission of Ho[3+] may be used in photodynamic therapy for the cancer treatment[28–30]. The Dy[3+] ions have been also used as an excellent sensitizer in different hosts[31,32]. Fu et al. successfully prepared the $K_3YB_6O_{12}$:Dy[3+], Eu^{3+} phosphor by solid state reaction method and have reported Dy[3+] ion to behave as a sensitizer and transfer a part of its excitation energy to the Eu^{3+} ions[33]. Zhang et al. synthesized rare earth and transition metal combination (Ho[3+]/Bi[3+]) co-doped $LaNbTiO_6$ phosphor via a facile sol–gel as well as combustion methods[34]. They found an energy transfer from Bi[3+] to Ho[3+] ions and blue to green color tunability. Recently, Guan et al. reported the Dy[3+], Ho[3+] co-doped $NaGdF_4$ nanophosphor and studied energy transfer from Dy[3+] to Ho[3+] ion under 360 nm excitations[35]. They found color tunable emission in narrow region from blue to weak green with color coordinates to vary from (0.26, 0.33) to (0.27, 0.36). Therefore, we need to broad the color tunable region, which lie from whitish to deep green via greenish yellow. For this we choose Dy[3+]/Ho[3+] co-doped $CaTiO_3$ and studied the energy transfer, color tunability and temperature dependent photoluminescence in detail, which has not been studied till now to the best of our knowledge.

In the present work, we have prepared Dy[3+], Ho[3+] singly doped and Dy[3+]/Ho[3+] co-doped $CaTiO_3$ phosphors by solid state reaction method at 1473 K. The structural and morphological properties were studies by XRD, FE-SEM and EDX measurements. The vibrational bands due to different groups present in phosphor were analyzed by FTIR measurements. It is found that whereas Ho[3+] emits intense green emission and weak red, Dy[3+] gives intense blue and yellow emissions on UV excitation. We optimized the concentrations of Dy[3+] and Ho[3+] ions separately in this host to get maximum photoluminescence intensities. All the colors are emitted in Dy[3+]/Ho[3+] co-doped $CaTiO_3$ on UV excitations, which are color tunable with concentrations. It is also found that an energy transfer takes place from Dy[3+] to Ho[3+] on excitation with 367 nm in $CaTiO_3$:4Dy[3+]/yHo[3+] phosphors and from Ho[3+] to Dy[3+] on excitation with 362 nm in $CaTiO_3$:3Ho[3+]/xDy[3+] phosphors. The energy transfer efficiency and interaction involved have been studied in the two cases. The CIE coordinates calculations show that this phosphor emits white light and tunable greenish yellow to deep green color light with the variation in the concentration of Dy[3+] and Ho[3+] ions. The lifetime of $^4F_{9/2}$ level of Dy[3+] and $^5S_2$ level of Ho[3+] ions have been also measured in the absence and presence of Ho[3+] and Dy[3+] ions, respectively. The temperature dependent photoluminescence studies have been carried out to check the thermal stability behavior of the $CaTiO_3$:4Dy[3+]/2Ho[3+] phosphor. Thus, Dy[3+], Ho[3+] singly doped and Dy[3+]/Ho[3+] co-doped $CaTiO_3$ phosphor materials may be useful in achieving multi-color display devices, n-UV chip excited LED/WLED's and in photodynamic therapy for the cancer treatments.

Results and discussion
Structural and morphological characterization
XRD measurements
The X-ray diffraction patterns of the pure $CaTiO_3$, $CaTiO_3$:4Dy[3+], $CaTiO_3$:3Ho[3+] and $CaTiO_3$:4Dy[3+]/2Ho[3+] phosphor samples were monitored in the 2θ range of 20-80° and it is shown in Fig. 1a–d along with its JCPDS file no—220153. The $CaTiO_3$ host has orthorhombic phase and its space group is Pnma(62). All the doped phosphors show sharp diffraction peaks which are confirm highly crystalline nature of the phosphors. There is no additional diffraction peaks found by doping of 4Dy[3+], 3Ho[3+] and 4Dy[3+]/2Ho[3+] in pure $CaTiO_3$. Therefore, addition of 4Dy[3+], 3Ho[3+] and 4Dy[3+]/2Ho[3+] ions in $CaTiO_3$ donot affects the phase of the $CaTiO_3$. Though doping of these ions at Ca^{2+} site, shift the diffraction peaks slightly towards higher 2θ angle side. This can be understood on the basis of their ionic radii. The ionic radii of Dy[3+], Ho[3+] and Ca^{2+} ions are 0.091, 0.090 and 0.100 nm, respectively. Therefore, on doping of Dy[3+], Ho[3+] ions at Ca^{2+} sites, crystal cell shrinks slightly due to which XRD peaks are shifted towards higher 2θ angle side. The effect of these shift for (121) peak is shown in Fig. 1e.

The value of average crystallite size (D) of pure $CaTiO_3$, $CaTiO_3$:4Dy[3+], $CaTiO_3$:3Ho[3+] and $CaTiO_3$:4Dy[3+]/2Ho[3+] phosphors were calculated with the help of Debye–Scherrer (D–S) equation[36]:

$$D = \frac{k\lambda}{\beta \cos\theta}, \qquad (1)$$

where D is the crystallite size, k is the shape factor (0.89), λ is the X-ray wavelength, β is the full width at half maximum (FWHM) and θ is the diffraction angle. The average crystallite size values were found to be 30.0, 31.42, 32.12 and 31.70 nm for the pure $CaTiO_3$, $CaTiO_3$:4Dy[3+], $CaTiO_3$:3Ho[3+] and $CaTiO_3$:4Dy[3+]/2Ho[3+] phosphors, respectively.

The micro-strain (e) has been also calculated for pure $CaTiO_3$, $CaTiO_3$:4Dy[3+], $CaTiO_3$:3Ho[3+] and $CaTiO_3$:4Dy[3+]/2Ho[3+] phosphors by using the relation:

$$e = \frac{\beta}{4 \tan\theta}, \qquad (2)$$
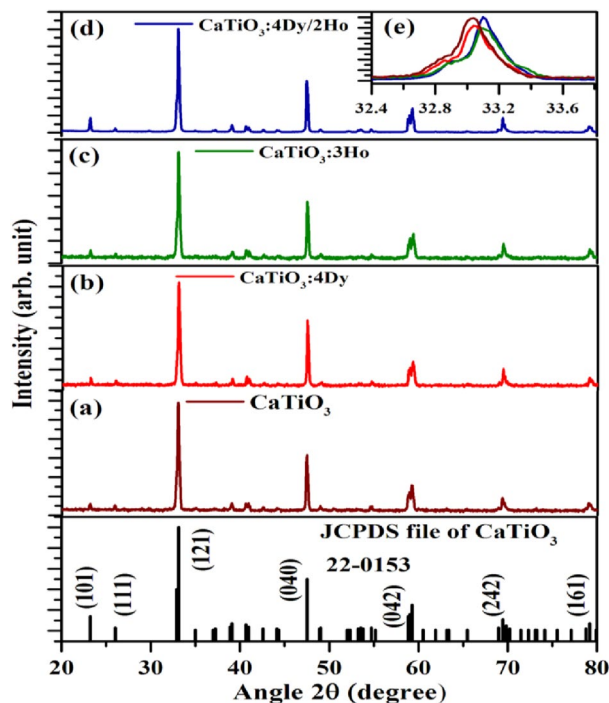
Figure 1. XRD patterns of (**a**) $CaTiO_3$, (**b**) $CaTiO_3$:$4Dy^{3+}$, (**c**) $CaTiO_3$:$3Ho^{3+}$ and (**d**) $CaTiO_3$: $4Dy^{3+}/2Ho^{3+}$ phosphors (**e**) Zoomed XRD patterns in 32.4–33.8º range.

where the terms have their usual meaning. The micro-strain values for pure $CaTiO_3$, $CaTiO_3$:$4Dy^{3+}$, $CaTiO_3$:$3Ho^{3+}$ and $CaTiO_3$:$4Dy^{3+}/2Ho^{3+}$ phosphors were found to be 6.1×10^{-5}, 5.6×10^{-5}, 5.3×10^{-5} and 5.9×10^{-5}, respectively.

FE-SEM and EDX measurements
The surface morphology of $CaTiO_3$:$4Dy^{3+}$, $CaTiO_3$:$3Ho^{3+}$ and $CaTiO_3$:$4Dy^{3+}/2Ho^{3+}$ phosphors are given in Fig. 2a–c, respectively. From the figure it is clear that particles are nearly spherical in shape and some particles are agglomerated with each other.

The average particles size of the $CaTiO_3$:$4Dy^{3+}$, $CaTiO_3$:$3Ho^{3+}$ and $CaTiO_3$:$4Dy^{3+}/2Ho^{3+}$ phosphors were calculated by histogram plots using image j software [see Fig. 2d–f)] and the values obtained are 0.35, 0.41 and 0.39 μm, respectively. Chauhan et al. have calculated the average particles size by SEM images in which some particles are agglomerated. They have used image j software and the histogram plot method for calculate average particles size[37]. Our group have also used image j software and histogram plot method for calculate average particles size from the SEM images[38].

The elements present in the prepared phosphors were verified by energy dispersive X-ray spectroscopic (EDX) measurements. Figure 3a–c shows the EDX patterns of $CaTiO_3$:$4Dy^{3+}$, $CaTiO_3$:$3Ho^{3+}$ and $CaTiO_3$:$4Dy^{3+}/2Ho^{3+}$ phosphors, respectively. The EDX spectra show the presence of Ca, Ti, O, Dy and Ho elements in the phosphors. The Dy and Ho peaks are very weak appear in the EDX spectra due to its low concentrations. Several researchers also reported the EDX spectra in which the concentration of do-pants are low and due to this its peak appear very weak in EDX spectra[38–40].

Optical characterization
Fourier transform infrared spectra (FTIR)
The FTIR spectra of the samples were used to categorize the vibrational bands due to different molecular groups present in the phosphor samples. The FTIR spectra of the different samples in the spectral range 400–3000 cm^{-1} are shown in the Fig. 4. The vibrational bands are observed at 433 and 541 cm^{-1}, which corresponds to Ca-O and Ti–O groups[2,3].

Photoluminescence excitation and emission spectra of $CaTiO_3$:xDy^{3+} phosphors
The PL excitation spectra of $CaTiO_3$:xDy^{3+} (where x = 3.0, 4.0 & 5.0 mol %) phosphor samples in the spectral region 300–475 nm with $\lambda_{em} = 573$ nm are shown in Fig. 5a. The PL excitation spectra show a number of peaks due to different transitions of Dy^{3+}. The peaks of Dy^{3+} ions situated at 352, 367, 388, 430 and 460 nm, which could be assigned to arise due to $^6H_{15/2} \rightarrow ^6P_{7/2}$, $^6H_{15/2} \rightarrow ^6P_{5/2}$, $^6H_{15/2} \rightarrow ^4I_{13/2}$, $^6H_{15/2} \rightarrow ^4G_{11/2}$ and $^6H_{15/2} \rightarrow ^4I_{15/2}$ transitions, respectively. The peaks at 352, 367 and 388 nm are intense compared to other peaks[1,41–43]. All these peaks wavelength lie in the emission range of n-UV LED chip. These peaks are therefore useful for LEDs applications.
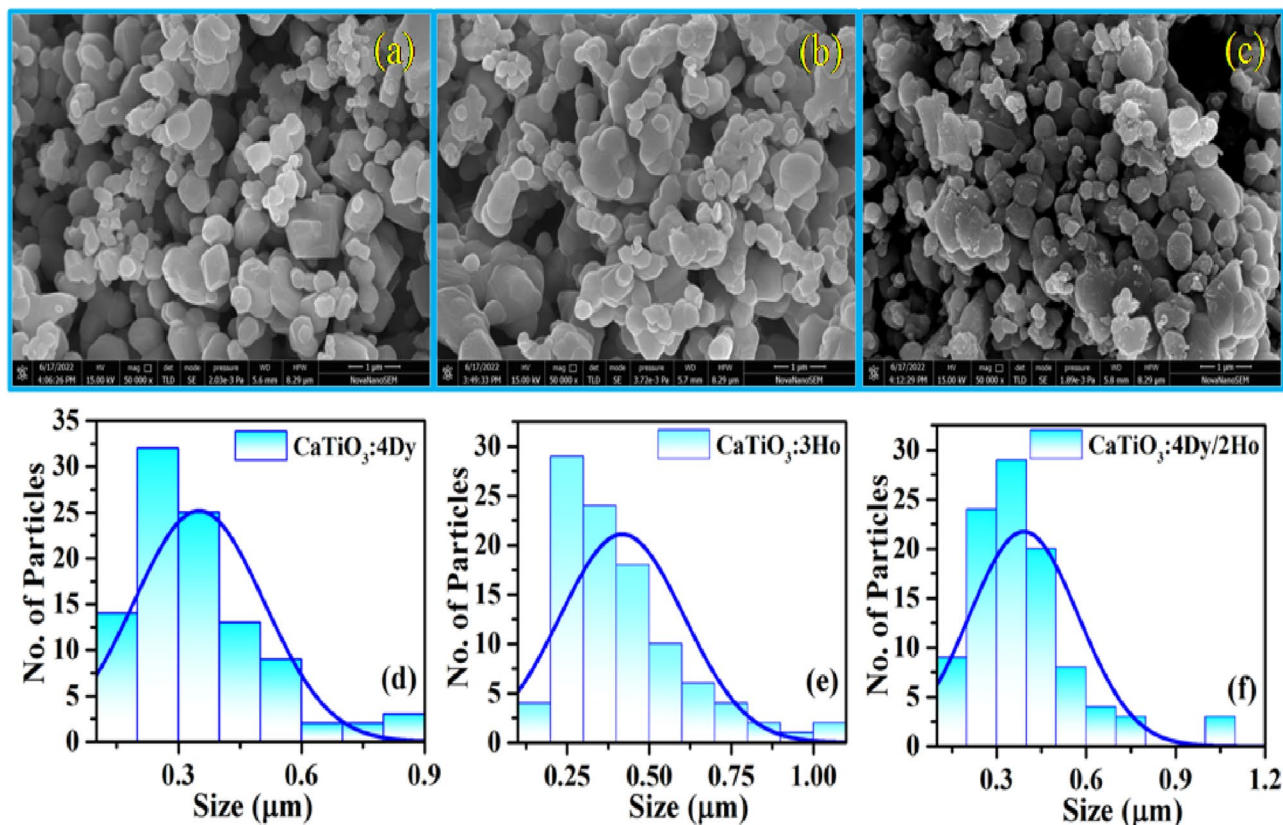
Figure 2. FE-SEM images of (**a**) CaTiO$_3$:4Dy^{3+}, (**b**) CaTiO$_3$:3Ho^{3+}, (**c**) CaTiO$_3$:4Dy^{3+}/2Ho^{3+} and histogram plots for particles size distribution of (**d**) CaTiO$_3$:4Dy^{3+}, (**e**) CaTiO$_3$:3Ho^{3+} and (**f**) CaTiO$_3$: 4Dy^{3+}/2Ho^{3+} phosphors.

The PL emission spectra of CaTiO$_3$:xDy^{3+} phosphors on excitation with 352 and 367 nm wavelengths in the spectral region 450–625 nm are shown in Fig. 5b,c, respectively. The emission spectra contain two intense peaks at 480 and 573 nm due to $^4F_{9/2} \rightarrow {}^6H_{15/2}$ and $^4F_{9/2} \rightarrow {}^6H_{13/2}$ transitions, respectively[43–45]. The 573 nm peak is more intense than 480 nm peak. The intensity of emission is highest for 4 mol % concentration of Dy^{3+} ion (see inset in Fig. 5b). The intensity of the peaks decreases for higher concentrations due to concentration quenching. The emission intensity is larger for 352 nm excitation.

Photoluminescence excitation and emission spectra of CaTiO$_3$:yHo^{3+} phosphors

Figure 6a shows the photoluminescence excitation (PLE) spectra of the yHo^{3+} (where y = 1.0, 3.0 & 5.0 mol %) doped CaTiO$_3$ phosphors in the spectral region of 300–500 nm with λ_{em} fixed at 547 nm (corresponding to the $^5S_2 \rightarrow {}^5I_8$ transition of Ho^{3+} ion). The spectra contain intense excitation peaks at 362, 419, 452 and 486 nm and they are assigned due to $^5I_8 \rightarrow {}^3H_5$, $^5I_8 \rightarrow {}^5G_5$, $^5I_8 \rightarrow {}^5G_6$ and $^5I_8 \rightarrow {}^3F_3$ transitions of Ho^{3+} ions, respectively[3,46]. The excitation peak at 452 nm due to $^5I_8 \rightarrow {}^5G_6$ transition appears with maximum intensity. The intensity of excitation peaks is optimum for 3 mol % of Ho^{3+} ions. Figure 6b–d show the PL emission spectra of the yHo^{3+} doped CaTiO$_3$ phosphors on excitations with 362, 419 and 452 nm in the spectral region 500–675 and 500–800 nm, respectively. The PL emission spectra contain an intense green alongwith weak red and very weak NIR bands at 539/547, 652 and 756 nm corresponding to $^5F_4/^5S_2 \rightarrow {}^5I_8$, $^5F_5 \rightarrow {}^5I_8$ and $^5S_2 \rightarrow {}^5I_7$ transitions of Ho^{3+} ions, respectively[3,46,47]. The intensity of green emission is dominated over the red and NIR emissions. The photoluminescence emission intensity is maximum at 3 mol % of Ho^{3+} ions concentration. For higher doping concentrations the emission intensity decrease due to concentration quenching effect (see inset of Fig. 6b). The PL emission intensity is largest for 452 nm excitation.

Photoluminesence excitation and emission spectra of CaTiO$_3$:4Dy^{3+}/yHo^{3+} phosphors

Photoluminescence excitation and emission spectra of CaTiO$_3$:4Dy^{3+} and CaTiO$_3$:3Ho^{3+} phosphors are shown in Fig. 7a,b, respectively. The transitions involved in the excitation and emission spectra are discussed earlier. Figure 7c shows the photoluminescence excitation and the emission spectra of CaTiO$_3$:4Dy^{3+}/2Ho^{3+} phosphor at λ_{em} = 547, 573 nm and λ_{ex} = 367 nm, respectively. The excitation peaks of Dy^{3+} and Ho^{3+} observed in mixed case (CaTiO$_3$:4Dy^{3+}/2Ho^{3+} phosphor) are exactly reproduced as in their individual cases. The 367 nm excitation in the mixed case gives blue and yellow as well as green emissions. This wavelength matches well with the level of Dy^{3+}. The appearance of emission from Ho^{3+} ion under 367 nm is partially due to excitation of Ho^{3+} ion (because Ho^{3+} ion also weakly excited by 367 nm) and the rest due to the energy transfer from Dy^{3+} to Ho^{3+} ions.
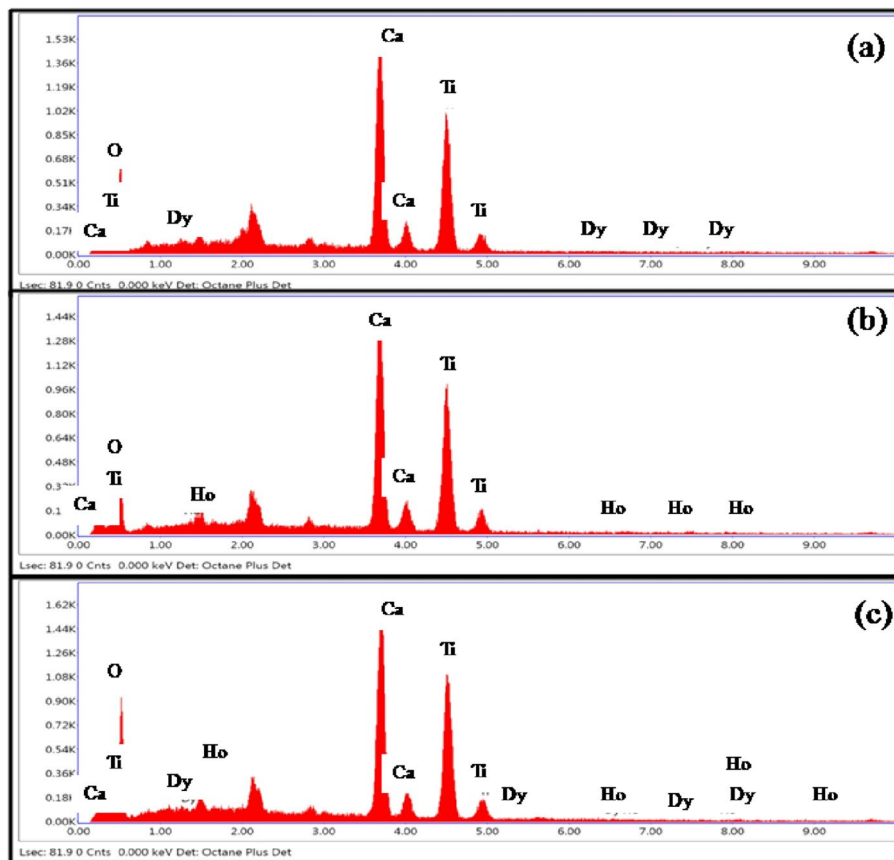
Figure 3. EDX spectra of (**a**) $CaTiO_3:4Dy^{3+}$, (**b**) $CaTiO_3:3Ho^{3+}$ and (**c**) $CaTiO_3: 4Dy^{3+}/2Ho^{3+}$ phosphor samples.
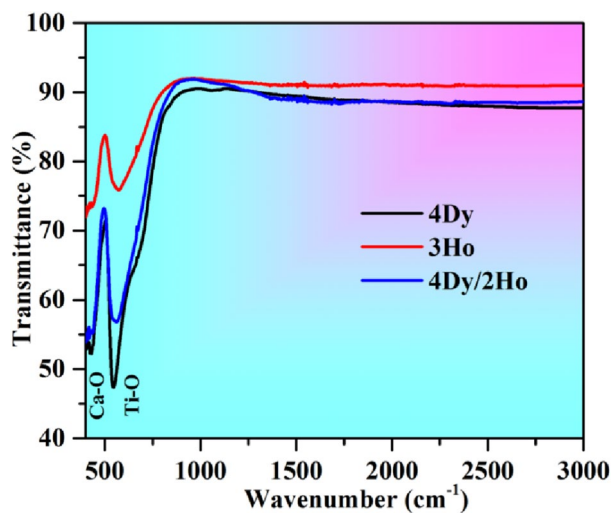
Figure 4. FTIR spectra of $CaTiO_3:4Dy^{3+}$, $CaTiO_3:3Ho^{3+}$ and $CaTiO_3:4Dy^{3+}/2Ho^{3+}$ phosphor samples.

A similar type spectra are also seen on excitation with 362 nm (a wavelength which match exactly with Ho^{3+} level) where the Dy^{3+} emission also appears with the Ho^{3+} emission [see Fig. 8b]. This shows that color emitted by the phosphor sample can be tuned by appropriate doping ratio of Dy^{3+}/Ho^{3+} ions in $CaTiO_3$ and selecting proper excitation wavelength.

The energy transfer from sensitizer to activator ions can occur when the excitation spectrum of the activator and emission spectrum of the sensitizer overlap on each other[48]. Figure 7a,b clearly shows that the exication peak
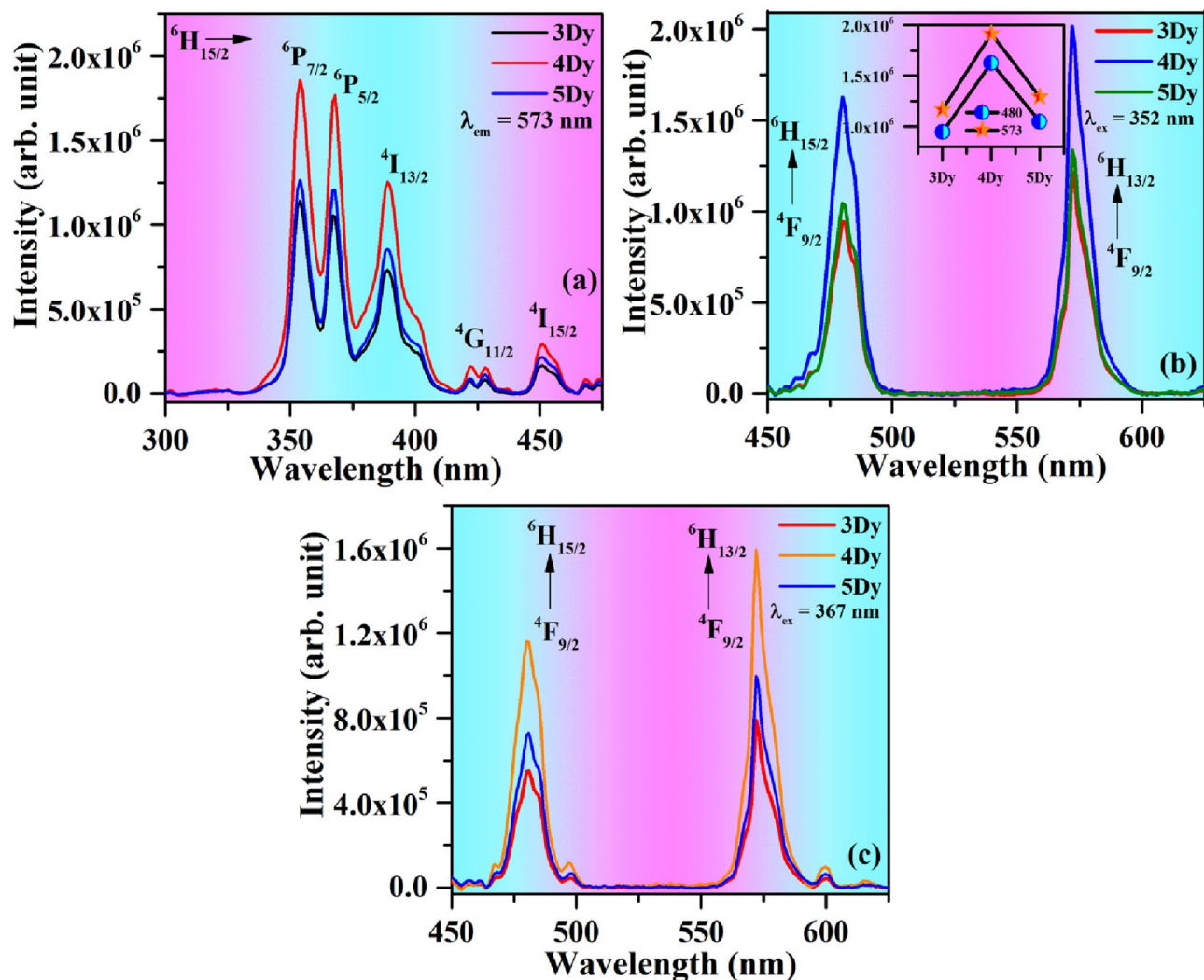
Figure 5. (**a**) Photoluminescence excitation (PLE) spectra of the xDy^{3+} doped $CaTiO_3$ phosphors by monitoring at $\lambda_{em} = 573$ nm. PL emission spectra of the xDy^{3+} doped $CaTiO_3$ phosphors with $\lambda_{ex} = $ (**b**) 352 and (**c**) 367 nm.

due to $^5I_8 \rightarrow {}^5F_3$ transition (486 nm) of Ho^{3+} ions overlap with the emission peak due to $^4F_{9/2} \rightarrow {}^6H_{15/2}$ transition (480 nm) of Dy^{3+} ions. This clearly indicates that an energy transfer is possible from Dy^{3+} to Ho^{3+} ions.

In order to understand the effect of Ho^{3+} ion concentrations on the photoluminescence intensity of Dy^{3+}, energy transfer efficiency and color tunability, we synthesized the $CaTiO_3:4Dy^{3+}/yHo^{3+}$ (where y = 0, 0.5, 1.0, 1.5, 2.0 & 3.0 mol%) phosphors, and monitored their photoluminescence emission spectra with $\lambda_{ex} = 367$ nm. The spectra obtained are shown in Fig. 8a. It can be seen that the PL emission intensity of Dy^{3+} ions decreased while that of Ho^{3+} ions increases with increasing the concentrations of Ho^{3+} ions and this is due to energy transfer from Dy^{3+} to Ho^{3+} ions. A reverse energy transfer (i.e. from Ho^{3+} to Dy^{3+} ions) is also possible for 362 nm excitation (due to overlapping of 362 nm band of Ho^{3+} and 367 nm band of Dy^{3+} [see Fig. 7c]). For this we co-doped xDy^{3+} (where x = 0, 1.0, 3.0 & 5.0 mol %) in $CaTiO_3:3Ho^{3+}$ phosphor and this is shown in Fig. 8b. The emission intensity of Ho^{3+} ions decrease with the increase of the concentration of Dy^{3+} ions. This clearly shows the energy transfer from Ho^{3+} to Dy^{3+} ions.

To understand the variation in emission intensity, the emission intensity of Ho^{3+} and Dy^{3+} ions with different concentrations of Ho^{3+} ions and fixed concentration of Dy^{3+} [i.e. $4Dy^{3+}/yHo^{3+}$ (where y = 0, 0.5, 1.0, 1.5, 2.0 & 3.0 mol%) co-doped $CaTiO_3$ phosphors] are shown in Fig. 9a,b). From the figure it is obvious that the emission intensity of Ho^{3+} ions increase while that of Dy^{3+} ion decrease with increasing the concentration of Ho^{3+} ions in $4Dy^{3+}/yHo^{3+}$ co-doped $CaTiO_3$ phosphors and it is maximum for 2 mol% of Ho^{3+} ions.

Energy transfer efficiency from Dy^{3+} to Ho^{3+} and Ho^{3+} to Dy^{3+} ions and nature of interaction

The energy transfer efficiency from Dy^{3+} to Ho^{3+} and Ho^{3+} to Dy^{3+} ions under 367 nm and 362 nm excitations can be calculated using the equation[4]:
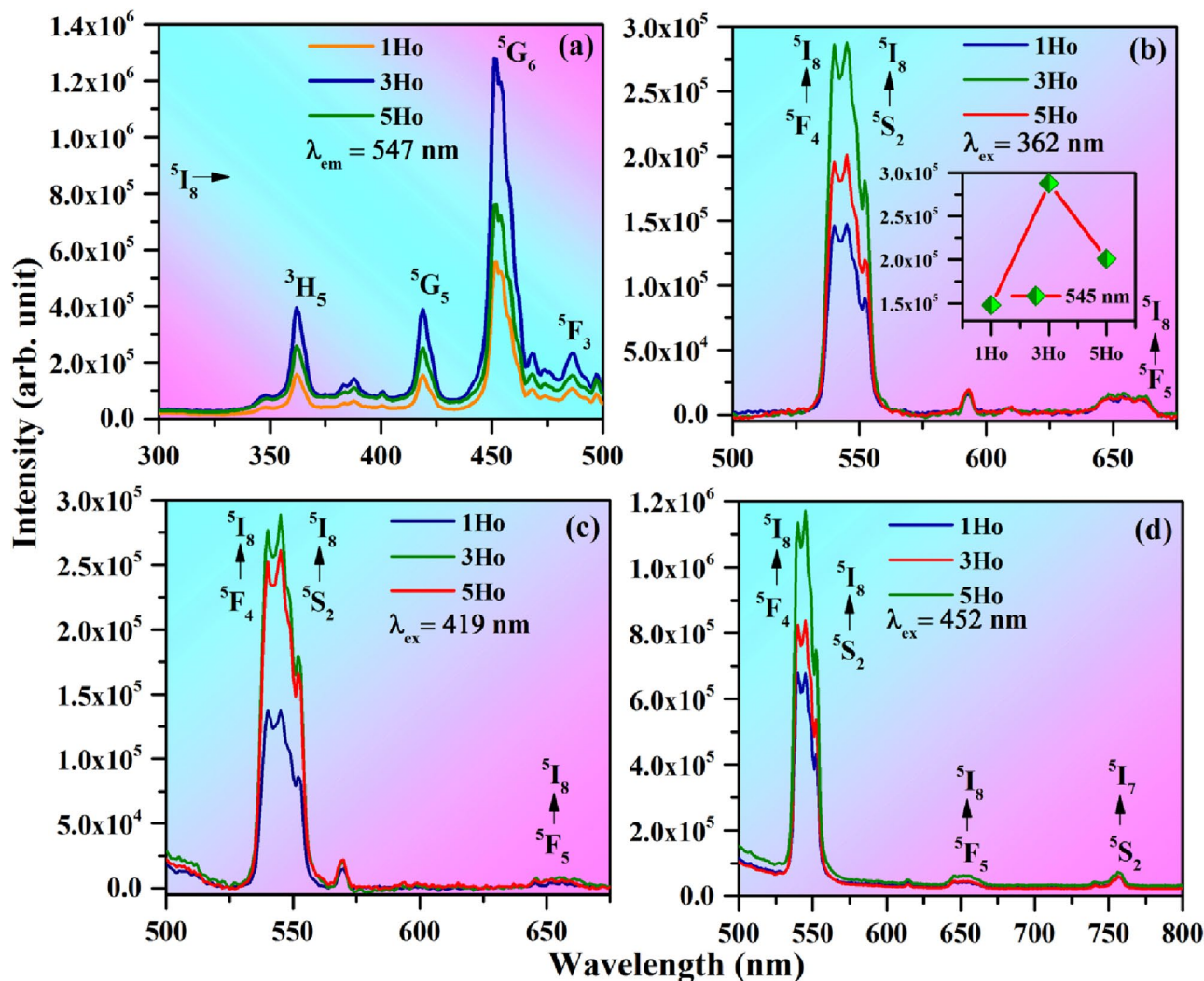
Figure 6. (**a**) Photoluminescence excitation (PLE) spectra of the yHo^{3+} doped CaTiO$_3$ phosphors by monitoring $\lambda_{em} = 547$ nm. PL emission spectra of the yHo^{3+} doped CaTiO$_3$ phosphors with (**b**) $\lambda_{ex} = 362$ nm, (**c**) $\lambda_{ex} = 419$ nm and (**d**) $\lambda_{ex} = 452$ nm.

$$\eta_T = \left(1 - \frac{I}{I_0}\right) \times 100\%, \qquad (3)$$

where I and I_0 are the emission intensities of sensitizer in the presence and absence of activator ion, respectively. Here, η_T represents the energy transfer efficiency. Under the 367 nm excitation the energy transfer efficiency with different Ho^{3+} ion concentrations is shown in Fig. 10. The value of energy transfer efficiency is 0, 13.55, 23.66, 36.32, 44.6 and 67.76% for CaTiO$_3$:4Dy^{3+}/yHo^{3+} (where y = 0, 0.5, 1.0, 1.5, 2.0 & 3.0 mol%) phosphors.

The energy transfer efficiency has been also calculated in the case of CaTiO$_3$:3Ho^{3+}/xDy^{3+} (where x = 0, 1.0, 3.0 & 5.0 mol%) phosphors under 362 nm excitation and the values are 0, 36.42, 59.56 and 69.39%, respectively.

Generally, the energy transfer from sensitizer (donor) to activator (acceptor) ions can be studied by the Förster's (FRET)/Dexter's theories in organic and inorganic materials[19,20]. These studied have many pros and cons in the advanced material design for different applications. The FRET usually observed in organic materials design and use in cell biology, medicine, WLED etc[19,49,50]. The energy transfer efficiency in FRET depends upon refractive index of solvent, dipole orientation and quantum yield of the donor etc[19]. However, Dexter's theory usually used to understand the non-radiative energy transfer due to exchange or multipolar interaction in oxide phosphors[21]. If the value of critical distance less than 5 Å, it is exchange interaction. However, if the value of critical distance is greater than 5 Å, it is multipolar interaction. In order, to understand the energy transfer interaction from sensitizer (Dy^{3+}) to activator (Ho^{3+}) ions in the CaTiO$_3$:4Dy^{3+}/yHo^{3+} phosphors, the value of critical distance needs to be evaluated. The value of critical distance between Dy^{3+}-Ho^{3+} ions could be calculated by using the relation[51]:

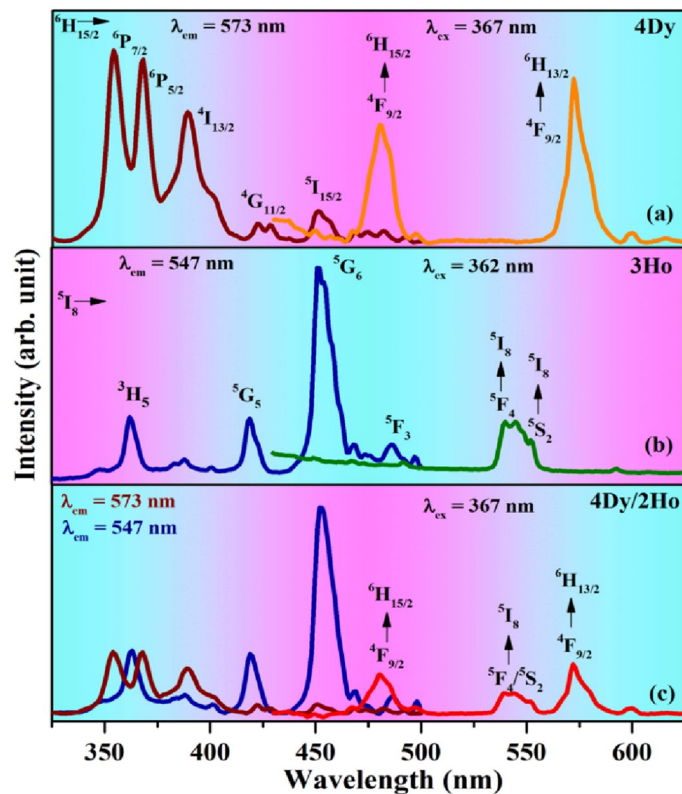$$R_c = 2\left[\frac{3V}{4\pi xN}\right]1/3, \qquad (4)$$

Figure 7. Photoluminescence excitation and emission spectra of (**a**) $CaTiO_3$:4Dy^{3+}, (**b**) $CaTiO_3$:3Ho^{3+} and (**c**) $CaTiO_3$:4Dy^{3+}/2Ho^{3+} phosphors.

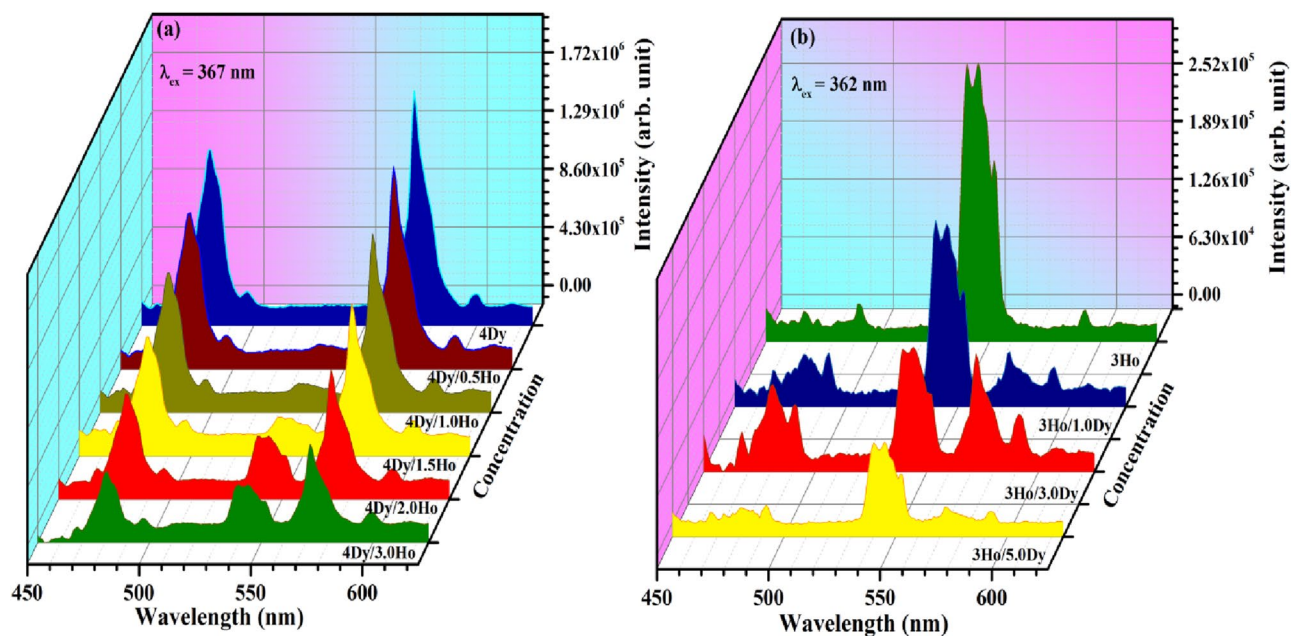**Figure 8.** Photoluminescence emission (PL) spectra of (**a**) $CaTiO_3$:4Dy^{3+}/yHo^{3+} (where y = 0, 0.5, 1.0, 1.5, 2.0 & 3.0 mol %) phosphors with λ_{ex} = 367 nm and (**b**) $CaTiO_3$:3Ho^{3+}/xDy^{3+} (where x = 0, 1.0, 3.0 & 5.0 mol %) phosphors with λ_{ex} = 362 nm.
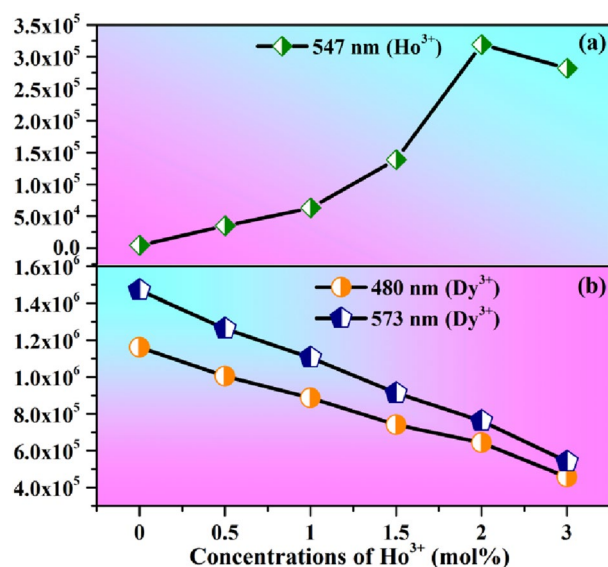
Figure 9. (**a,b**) Variation in emission intensities of Ho^{3+} and Dy^{3+} ions bands with the variation of concentrations of Ho^{3+} ion in CaTiO$_3$:4Dy^{3+}/yHo^{3+} phosphors under 367 nm excitation.
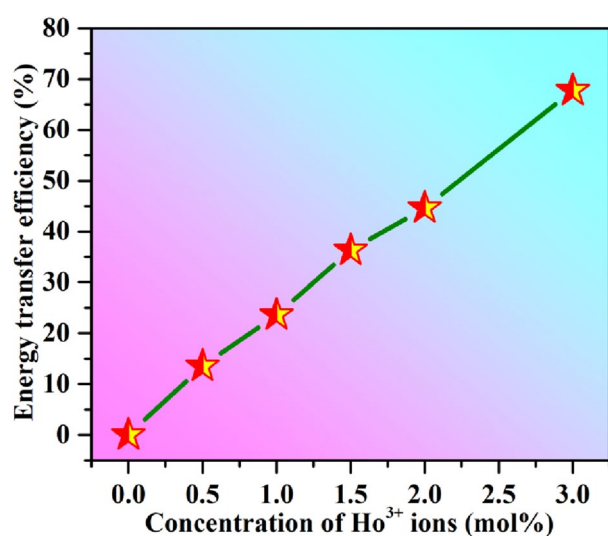
Figure 10. Energy transfer efficiency from Dy^{3+} to Ho^{3+} ion in CaTiO$_3$:4Dy^{3+}/yHo^{3+} (where y = 0.0, 0.5, 1.0, 1.5, 2.0 & 3.0 mol %) phosphors.

where V is the volume of the unit cell, N is the number of Ca site. The critical concentration x is defined as the total concentration of Dy^{3+} and Ho^{3+} ions, when the emission intensity of Dy^{3+} with Ho^{3+} is half of that without Ho^{3+} doping. Here in, x is approximately ~ 0.063, V = 224.0342 Å^3 and N = 4. The calculated value of R$_c$ is found to be 11.44 Å. This value is greater than 5 Å which indicates that the energy transfers from sensitizer (Dy^{3+}) to activator (Ho^{3+}) ion is due to multipolar interaction. Dwivedi et al. have also studied the energy transfer from Ho^{3+} to Eu^{3+} in Ca$_{0.05}$Y$_{1.93-x}$O$_2$ host. They have reported the value of critical distance is 15.14 Å and have calculated the multipolar interaction by Dexter's formula and Reisfield's approximation[4].

The multipolar interaction can be determined by Dexter's formula for energy transfer and Reisfield's approximation[52]:

$$\frac{I}{I_0} = C^{n/3}, \qquad (5)$$

where I and I$_0$ are the emission intensities of Dy^{3+} peak in the absence and presence of Ho^{3+} ions. C is the critical concentrations of Dy^{3+} and Ho^{3+} ions and n = 6, 8 and 10 for dipole–dipole (d–d), dipole–quadrupole (d–q) and quadrupole–quadrupole (q–q) interactions, respectively. The plot of I/I$_0$ versus concentration are given in Fig. 11. A better fitting is observed for n = 10. Hence, the energy transfers from Dy^{3+} to Ho^{3+} ions is due
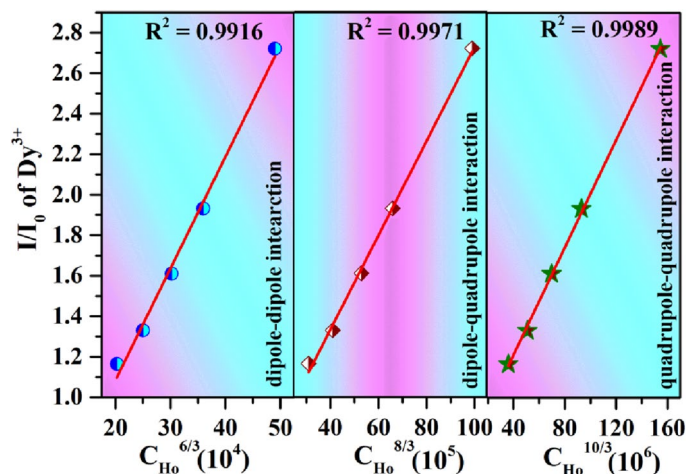
Figure 11. Plots of I/I_0 vs $C^{n/3}$ (where n = 6, 8 & 10) for $CaTiO_3:4Dy^{3+}/yHo^{3+}$ phosphors.

to the quadrupole–quadrupole (q-q) interactions. This interaction in the case of energy transfer from Ho^{3+} to Dy^{3+} is found to be due to dipole–dipole.

Energy level diagram of Dy^{3+}, Ho^{3+} ions and the mechanism of energy transfer from Dy^{3+} to Ho^{3+} ions/Ho^{3+} to Dy^{3+} ions

The excitation and emission spectra of Dy^{3+} and Ho^{3+} ions in Figs. 5 and 6 can be understood easily on the basis of energy level diagram shown in Fig. 12. The Dy^{3+} ions present in the ground state ($^6H_{15/2}$), on excitation with 352 and 367 nm it promoted to the $^6P_{7/2}$ and $^6P_{5/2}$ excited states, respectively. The excited Dy^{3+} ions from $^6P_{7/2}$ and $^6P_{5/2}$ state populate the lowest excited $^4F_{9/2}$ state through several non-radiative relaxation processes. From $^4F_{9/2}$ state, Dy^{3+} ions give emissions at 480 (blue) and 573 nm (yellow) by $^4F_{9/2} \rightarrow {}^6H_{15/2}$ and $^4F_{9/2} \rightarrow {}^6H_{13/2}$ transitions, respectively.

Similarly, the Ho^{3+} ions in ground state ($^5I_8$), on excitation with 362, 419 and 452 nm are promoted to the $^3H_5$, $^5G_5$ and $^5G_6$ excited states, respectively. The excited Ho^{3+} ions from these states relax to the $^5F_4/^5S_2$ and $^5F_5$ states. The Ho^{3+} ions from $^5F_4/^5S_2$ states give strong green emissions at 539 and 547 nm through $^5F_4/^5S_2 \rightarrow {}^5I_8$ transitions. The ions in $^5S_2$ state also give emission in NIR region at 756 nm due to $^5S_2 \rightarrow {}^5I_7$ transition. The $^5F_5$
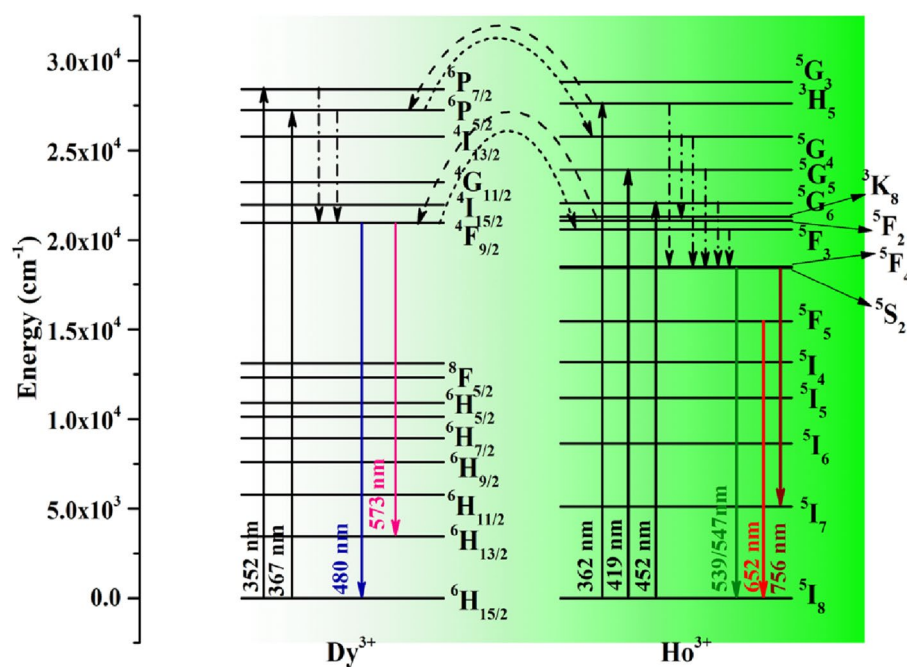

Figure 12. Schematic energy level diagrams of Dy^{3+}, Ho^{3+} ions and energy transfer mechanism involved from Dy^{3+} to Ho^{3+} and Ho^{3+} to Dy^{3+} ions in photoluminescence process.

state also populated through non-radiative relaxation from $^5F_4/^5S_2$ states gives relatively a weak red emission at 652 nm due to $^5F_5 \rightarrow {}^5I_8$ transition of Ho^{3+} ion.

However, when Dy^{3+} and Ho^{3+} both ions are present in the sample simultaneously, an energy transfer takes place from Dy^{3+} to Ho^{3+} ions on 367 nm excitation due to which emission intensity of Ho^{3+} bands increased and that of Dy^{3+} decreased. The energy transfer mechanism from Dy^{3+} to Ho^{3+} ions can be understood though the energy level diagram shown in the Fig. 12. Actually when Ho^{3+} ions are co-doped in $CaTiO_3$:Dy^{3+} phosphor, a part of energy is transferred from $^6P_{5/2}$ state of Dy^{3+} to $^5G_4$ state of Ho^{3+} ions under 367 nm excitations. The Ho^{3+} ions from $^5G_4$ excited state relax non radiatively to the $^5F_4/^5S_2$ excited states and give green emission at 539/547 nm due to $^5F_4/^5S_2 \rightarrow {}^5I_8$ transitions. Another possibility of energy transfers from Dy^{3+} to Ho^{3+} may be that the excited Dy^{3+} ions from $^6P_{5/2}$ state relax non radiatively to $^4F_{9/2}$ (lowest excited state) and transfer a part of its excitation energy from this state to the $^5F_3$ state of Ho^{3+} ion and loose another part radiatively to give radiative transitions $^4F_{9/2} \rightarrow {}^6H_{15/2}$ (blue) and $^4F_{9/2} \rightarrow {}^6H_{13/2}$ (yellow) with smaller intensity. The excited Ho^{3+} ions in $^5F_3$ state relax non-radiatively to the $^5F_4/^5S_2$ states which finally gives green emission.

As we have mentioned earlier, on excitation with 362 nm, a reverse energy transfer (i.e. from Ho^{3+} to Dy^{3+} ions) occurs and the mechanism involved can be understood again on the basis of energy level diagram shown in Fig. 12. Ho^{3+} ions transfer a part of their excitation energy from $^3H_5$ state (Ho^{3+}) to $^6P_{5/2}$ state (Dy^{3+}) under 362 nm excitations in $CaTiO_3$:$3Ho^{3+}$/xDy^{3+} phosphors. The Dy^{3+} ions from this state relax non-radiatively to the $^4F_{9/2}$ excited state and give blue and yellow emissions. Another possibility of energy transfer from Ho^{3+} to Dy^{3+} is that the excited Ho^{3+} ions from $^3H_5$ state relax non radiatively to $^5F_2$ state and from there Ho^{3+} ions transfer a part of their excitation energy to the $^4F_{9/2}$ state of Dy^{3+} ion. Thus, on excitation with 367/362 nm, we get bands due to Dy^{3+} as well as Ho^{3+} both ions via energy transfer from Dy^{3+} to Ho^{3+} ions and vice versa.

Color coordinates, CCT and color purity calculations

As we have seen that the Ho^{3+} doped $CaTiO_3$ emits intense green, weak red and NIR emissions. Whereas, Dy^{3+} doped $CaTiO_3$ sample emits blue and yellow emissions. So if both the rare earth ions are doped together in $CaTiO_3$ host, it gives multicolor emission on excitation with 362/367 nm wavelengths. The CIE (commission Internationale de I'Eclairage) diagram is an excellent tool to verify the multicolor emitted from the doped/co-doped phosphors[2]. When only Dy^{3+} ions are present in the $CaTiO_3$, the CIE coordinates lie in whitish region on excitation with 367 nm. However, if yHo^{3+} co-doped in $CaTiO_3$:$4Dy^{3+}$ phosphor, the color coordinates vary from whitish to greenish yellow region. On the other hand, $CaTiO_3$:$3Ho^{3+}$ phosphor gives intense green emission. The color coordinates vary from deep green to greenish yellow in $CaTiO_3$:$3Ho^{3+}$/xDy^{3+} phosphors under the 362 nm excitation. Figure 13a,b shows the CIE diagram of $CaTiO_3$:$4Dy^{3+}$/yHo^{3+} and $CaTiO_3$:$3Ho^{3+}$/xDy^{3+} phosphors under 367 and 362 nm excitation wavelengths, respectively.

It is interesting to observe that $CaTiO_3$:$4Dy^{3+}$/yHo^{3+} phosphors show excellent color tunability from whitish to green through greenish yellow under 362 nm excitation. Figure 14a,b shows the PL spectra and the CIE diagram for $CaTiO_3$:$4Dy^{3+}$/yHo^{3+} phosphors with $\lambda_{ex} = 362$ nm. The green emission intensity increased with increasing the Ho^{3+} ion concentration and the intensity of blue and yellow (Dy^{3+} ions) decreased. This occurs due to sharing of excitation energy in between Ho^{3+} and Dy^{3+} both ions. Thus for 0 mol% doping of Ho^{3+} in $CaTiO_3$:$4Dy^{3+}$/yHo^{3+} phosphors, the emission color lies in whitish region (due to pure Dy^{3+}) with CIE coordinates (0.33, 0.38). When the Ho^{3+} concentrations in $CaTiO_3$:$4Dy^{3+}$/yHo^{3+} phosphors is increased from 0 to 3 mol %,
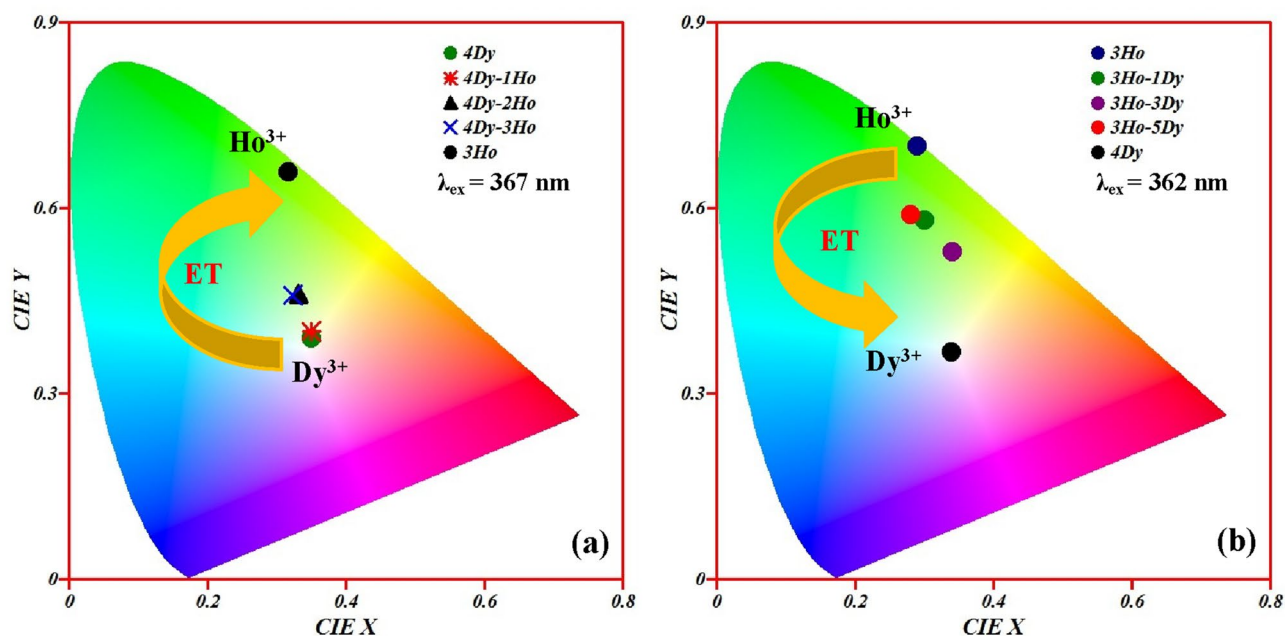

Figure 13. CIE diagram of (**a**) $CaTiO_3$:$4Dy^{3+}$/yHo^{3+} phosphors under 367 nm excitations and (**b**) $CaTiO_3$:$3Ho^{3+}$/xDy^{3+} phosphors under 362 nm excitation.

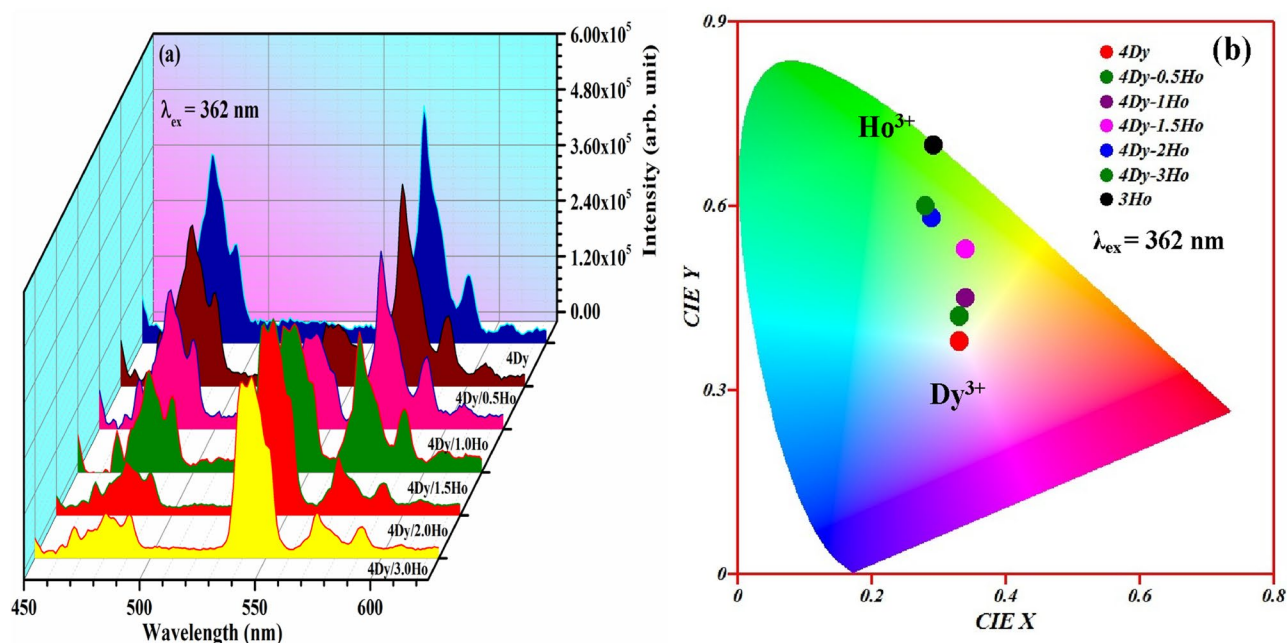**Figure 14.** (**a**) Photoluminescence emission spectra and (**b**) CIE diagram of $CaTiO_3$:$4Dy^{3+}$/yHo^{3+} phosphors under 362 nm excitations.

CIE coordinates of the phosphors is changed from whitish (0.33, 0.38) to green (0.28, 0.60). This is also obvious from emission spectra in Fig. 14a.

The values of CIE coordinates for different concentrations of Ho^{3+} are given in Table 1. A similar thing is observed in $CaTiO_3$:$3Ho^{3+}$/xDy^{3+} phosphors and the color coordinates are given in Table 1. The variation in CIE coordinates clearly show the possibility of achieving multicolor tunability by adjusting the Dy^{3+}/Ho^{3+} doping concentrations. Hence, Ho^{3+}/Dy^{3+} co-doped $CaTiO_3$ phosphors can be used in the field of single matrix perovskite tunable phosphor materials which are suitable for display devices, LED/WLEDs for solid state lighting applications.

The correlated color temperature (CCT) is used to evaluate the nature of emitted light from the phosphors i.e. whether it is warm, natural or cool white light. The CCT values are calculated using McCammys' equation[2, 52]:

$$T = -449(n^3) + 3525(n^2) - 6823.3(n) + 5520.33, \tag{6}$$

Phosphors	Wavelengths (nm)	CIE Coordinates	CCT values	Color purity
$4Dy^{3+}$	367	(0.35, 0.39)	4955	22.1
$4Dy^{3+}$/$1Ho^{3+}$	367	(0.35, 0.40)	4983	25.1
$4Dy^{3+}$/$2Ho^{3+}$	367	(0.33, 0.46)	5568	37.5
$4Dy^{3+}$/$3Ho^{3+}$	367	(0.32, 0.46)	5767	34.7
$3Ho^{3+}$	367	(0.33, 0.66)	5549	98.2
$3Ho^{3+}$	362	(0.29, 0.70)	6066	99.1
$3Ho^{3+}$/$1Dy^{3+}$	362	(0.30, 0.58)	6052	65.5
$3Ho^{3+}$/$3Dy^{3+}$	362	(0.34, 0.53)	5328	61.5
$3Ho^{3+}$/$5Dy^{3+}$	362	(0.28, 0.59)	6405	63.4
$4Dy^{3+}$	362	(0.33, 0.38)	5596	13.2
$4Dy^{3+}$/$0.5Ho^{3+}$	362	(0.33, 0.42)	5588	25.4
$4Dy^{3+}$/$1.0Ho^{3+}$	362	(0.34, 0.45)	5333	37.4
$4Dy^{3+}$/$1.5Ho^{3+}$	362	(0.34, 0.53)	5328	61.6
$4Dy^{3+}$/$2.0Ho^{3+}$	362	(0.29, 0.58)	6238	62.9
$4Dy^{3+}$/$3.0Ho^{3+}$	362	(0.28, 0.60)	6382	66.3

Table 1. CIE coordinates and CCT values of Dy^{3+}, Ho^{3+} and Dy^{3+}/Ho^{3+} co-doped $CaTiO_3$ phosphors under 362 and 367 nm excitation wavelengths.

where n = $(x – 0.3320)/(y – 0.1858)$ and (x, y) refers the CIE coordinates. The calculated CCT values are given in Table 1. The CCT values lie between natural and cool white light range.

The color purity of the phosphor materials is another important parameter to recognize it as a good source of light for a particular color for solid state lighting applications. The color purity of the light source can be calculated by following relation[52]:

$$\text{Color purity} = \frac{\sqrt{(x - x_i)^2 + (y - y_i)^2}}{\sqrt{(x_d - x_i)^2 + (y_d - y_i)^2}} \times 100\%, \tag{7}$$

where (x, y) are the CIE coordinates of the phosphor, (x_d, y_d) are the CIE coordinates of dominant wavelength and (x_i, y_i) are the CIE coordinates for standard white light source. The value of color purity is mentioned in the Table 1. The value of color purity varies from 13.2 to 66.3 for CaTiO$_3$:4Dy^{3+}/yHo^{3+} phosphors under 362 nm excitations.

Lifetime measurements

Lifetime study helps to understand the fundamental issues such as dopant location, surface defect etc. in the phosphor materials[53]. We have measured the lifetime of $^4F_{9/2}$ level of Dy^{3+} in the absence and presence of Ho^{3+} ions with λ_{ex} = 367 nm and λ_{em} = 480 nm and the decay curves are shown in Fig. 15a–d. We have also measured the lifetime of $^5S_2$ level of Ho^{3+} ion in the absence and presence of Dy^{3+} ion under λ_{ex} = 362 nm and λ_{em} = 547 nm and the decay curves are shown in Fig. 16a–d. It is found that all the decay curves fit well by single exponential formula[54]:

$$I(t) = I_0 \exp(-t/\tau), \tag{8}$$

where I_0 and $I(t)$ are the PL emission intensities at the time zero and at t seconds, respectively and 'τ' is the lifetime. It is interesting to note that even in co-doped cases the decay curves fit well with single exponential. If the decay curve needs multiexponential fitting, then probably there is defect also involved which must affect the lifetime of activator[55]. However, in our case even after the co-doping the decay curve fits well by single exponential. Therefore, we have concluded that there is no defect present in the materials. The values of lifetime are found to be 209, 197, 173 and 165 μs for 4Dy^{3+} doped and 4Dy^{3+}/1Ho^{3+}, 4Dy^{3+}/2Ho^{3+}, 4Dy^{3+}/3Ho^{3+} co-doped CaTiO$_3$ phosphors, respectively. However, the values of lifetime are found to be 27.11, 26.53, 25.40 and 24.60 μs for 3Ho^{3+} doped and 3Ho^{3+}/1Dy^{3+}, 3Ho^{3+}/3Dy^{3+}, 3Ho^{3+}/5Dy^{3+} co-doped CaTiO$_3$ phosphors, respectively. Thus, the lifetime for $^4F_{9/2}$ level of Dy^{3+} ion decreased in presence of Ho^{3+} ions, due to energy transfer from Dy^{3+} to Ho^{3+} ions and the lifetime for $^5S_2$ level of Ho^{3+} ion also decreased in presence of Dy^{3+} ions, due to energy transfer from Ho^{3+} to Dy^{3+} ions. Dwivedi et al. studied the downshifting and upconversion in Ho^{3+}/Yb^{3+} co-doped GdNbO$_4$

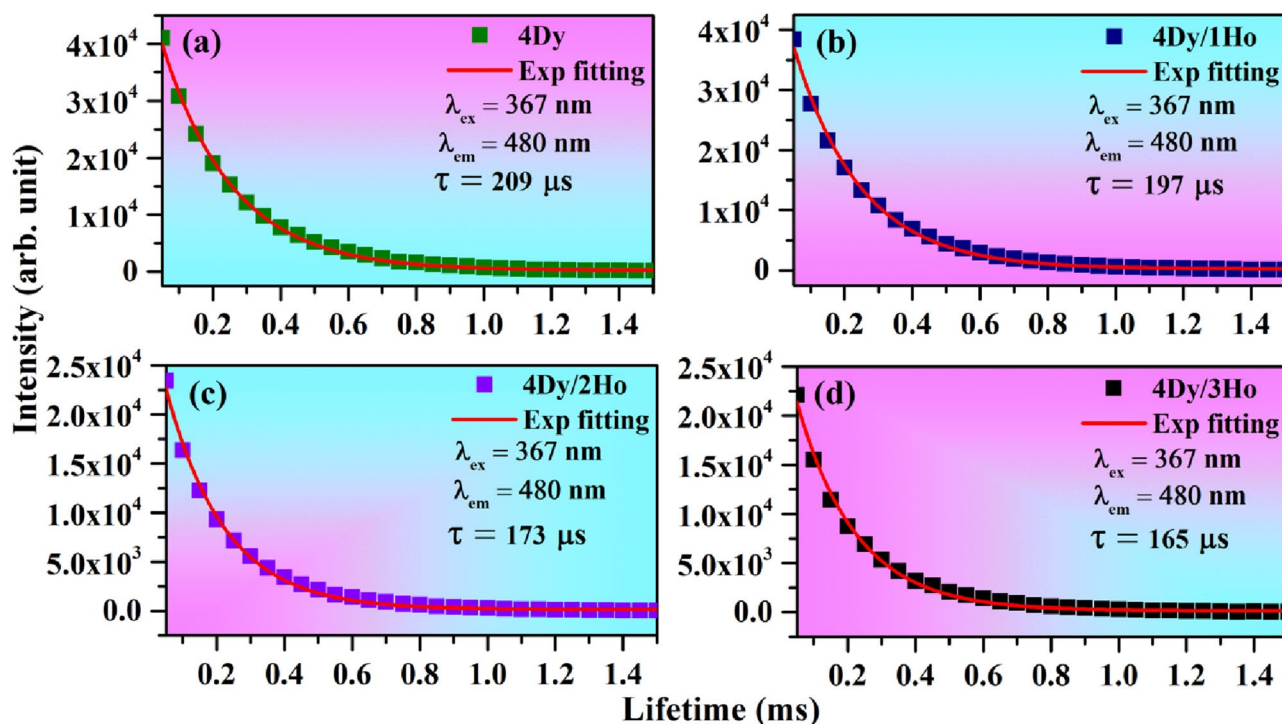**Figure 15.** Lifetime of $^4F_{9/2}$ level of Dy^{3+} in (**a**) 4Dy^{3+}, (**b**) 4Dy^{3+}/1Ho^{3+}, (**c**) 4Dy^{3+}/2Ho^{3+} and (**d**) 4Dy^{3+}/3Ho^{3+} co-doped CaTiO$_3$ with λ_{ex} = 367 nm and λ_{em} = 480 nm.
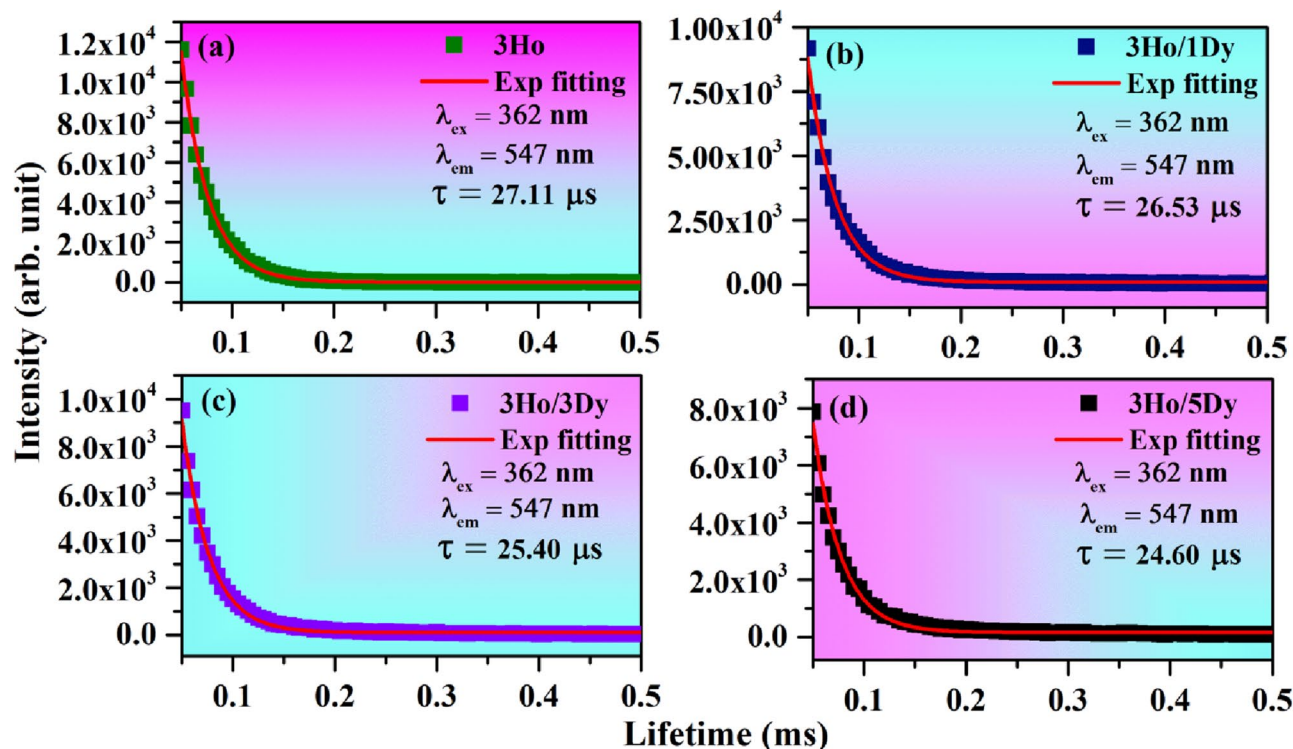
Figure 16. Lifetime of $^5S_2$ level of Ho^{3+} in (**a**) $3Ho^{3+}$, (**b**) $3Ho^{3+}/1Dy^{3+}$, (**c**) $3Ho^{3+}/3Dy^{3+}$ and (**d**) $3Ho^{3+}/5Dy^{3+}$ co-doped $CaTiO_3$ with $\lambda_{ex} = 362$ nm and $\lambda_{em} = 547$ nm.

phosphor. They have also reported the lifetime of Ho^{3+} in microsecond (μs) under 449 nm excitation and 540 nm emission wavelengths[56]. Mahata et al. also reported the lifetime of Ho^{3+} ions in microsecond[57].

Temperature dependent photoluminescence and photoluminescence quantum yield (PLQY) measurements

To know the thermal stability of the phosphor samples, we studied the temperature dependent photoluminescence emission spectra (TDPL) of $CaTiO_3$:$4Dy^{3+}$/$2Ho^{3+}$ phosphor in the temperature range 303–483 K with 367 nm excitation. The thermal stability is very important for the applications of phosphor in industrial fields. The temperature dependent normalized PL emission intensity for $CaTiO_3$:$4Dy^{3+}$/$2Ho^{3+}$ phosphor is depicted in Fig. 17a. As can be seen, the PL emission intensity decreased with the increase in temperature. This decrease in PL intensity is due to thermal quenching, which occurs due to non-radiative relaxation of phonons from higher excited states[4]. From Fig. 17a we found that the emission intensity at 423 K is 82% of 303 K for
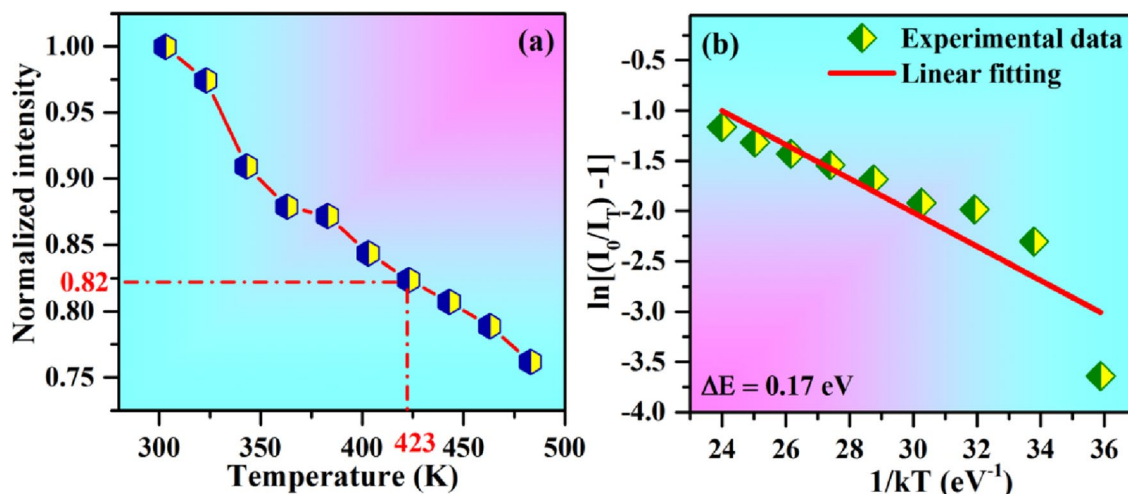

Figure 17. (**a**) An intensity plot as a function of temperature and (**b**) $\ln[(I_0/I_T)-1]$ vs $1/kT$ plot for $CaTiO_3$:$4Dy^{3+}$/$2Ho^{3+}$ phosphor.

$CaTiO_3$:4Dy^{3+}/2Ho^{3+} phosphor. Hence the loss in emission intensity is only 18% at 423 K. This clearly shows that this phosphor material is highly stable. We have compared the thermal stability of our materials with the thermal stability of other Dy^{3+} doped/co-doped materials and it is given in the Table 2. The obtained value of thermal stability in present study has been higher than the other reported values [see Table 2]. Hence, $CaTiO_3$:4Dy^{3+}/2Ho^{3+} phosphor shows good thermal stability and can be used for LED applications.

The activation energy for thermal quenching process is calculated by Arrhenius equation[63,64]:

$$\frac{I_T}{I_0} = \frac{1}{1 + Aexp\left(-\frac{\Delta E}{kT}\right)},$$

(9)

where I_0 is the initial emission intensity at 303 K, I_T is the emission intensity at temperature T K, ΔE is the activation energy, k is Boltzman constant (8.629×10^{-5} eV/K) and A is the constant frequency factor. The value of activation energy could be calculated from $\ln[(I_0/I_T) - 1]$ versus $1/kT$ plot and it is shown in Fig. 17b. The slope of the fitted line gives the value of activation energy. In the present case its value is found to be 0.17 eV for $CaTiO_3$:4Dy^{3+}/2Ho^{3+} phosphor. This clearly shows that this phosphor material is highly stable for various applications.

The photoluminescence quantum yield (PLQY) is an important parameter for the phosphor material to know its photoluminescence efficiency. The quantum yield is mathematically defined as the ratio of total number of photon emitted to the total number of photon absorbed under certain excitation[65,66].

The absolute photoluminescence quantum yield of $CaTiO_3$:4Dy^{3+}, $CaTiO_3$:4Dy^{3+}/2Ho^{3+} and $CaTiO_3$:3Ho^{3+} phosphors are monitored by using an integrating sphere with λ_{ex} = 367 and 452 nm, respectively. The value of PLQY is found to be 30%, 33% and 35% for $CaTiO_3$:4Dy^{3+}, $CaTiO_3$:4Dy^{3+}/2Ho^{3+} and $CaTiO_3$:3Ho^{3+} phosphors, respectively. We have compared the PLQY of our materials with PLQY of other Dy^{3+} doped/co-doped phosphors and it is given in the Table 3. The obtained value of PLQY in present study has been higher than the PLQY of other Dy^{3+} doped/co-doped phosphors [see Table 3]. Hence, $CaTiO_3$:4Dy^{3+}, $CaTiO_3$:4Dy^{3+}/2Ho^{3+} and $CaTiO_3$:3Ho^{3+} phosphors can be used for LED/WLED's applications.

Conclusions

In this study, Dy^{3+}, Ho^{3+} singly doped and Dy^{3+}/Ho^{3+} co-doped $CaTiO_3$ phosphor materials have been prepared by solid state reaction method at 1473 K. The prepared materials are characterized using structural and optical techniques. The phosphor samples show orthorhombic structure with Pnma(62) space group. The PL emission spectra of Dy^{3+} doped $CaTiO_3$ gives intense blue and yellow emissions, while the Ho^{3+} doped $CaTiO_3$ shows intense green emissions under UV LED wavelengths. A co-doping of the two ions together show an energy transfer from Dy^{3+} to Ho^{3+} as well as from Ho^{3+} to Dy^{3+} for $CaTiO_3$:4Dy^{3+}/yHo^{3+} and $CaTiO_3$:3Ho^{3+}/xDy^{3+} phosphors on λ_{ex} = 367 and 362 nm excitations, respectively. It is found that the energy transfers from Dy^{3+} to Ho^{3+} ion are due to quadruple-quadruple interaction whereas for Ho^{3+} to Dy^{3+} ion it is due to dipole–dipole.

Phosphor samples	Thermal stability (423 K)	References
$CaTiO_3$:4 mol%Dy^{3+}/2 mol%Ho^{3+}	82%	Present study
$BaLu_2Si_3O_{10}$: 0.04Dy^{3+}, 0.1Eu^{3+}	81.15%	[58]
$Ba_3Bi(PO_4)_3$:8at.%Dy^{3+},0.8at.%Eu^{3+}	70%	[59]
$LiMgBO_3$:0.03Tm^{3+}/0.05Dy^{3+}/0.05Li^+	61.5%	[60]
$Sr_3Gd(PO_4)_3$:3%Dy^{3+},6% Eu^{3+}	80%	[61]
$InNbTiO_6$:0.06Dy^{3+}	50%	[62]

Table 2. A comparison of the thermal stability for $CaTiO_3$:4Dy^{3+}/2Ho^{3+} phosphor with the thermal stability of other Dy^{3+} doped/co-doped phosphors.

Phosphor samples	PLQY (%)	References
$CaTiO_3$:3 mol%Ho^{3+}	35	Present study
$CaTiO_3$:4 mol%Dy^{3+}	30	Present study
$CaTiO_3$:4 mol%Dy^{3+}/2 mol%Ho^{3+}	33	Present study
$SrAl_2O_4$:1%Dy^{3+}	9.52	[65]
$InNbTiO_6$:0.06Dy^{3+}	23.4	[62]
$K_3Y(PO_4)_2$:2 mol%Dy^{3+}	13	[66]
$Na_3La(PO_4)_2$:2 mol%Dy^{3+}	11	[66]
$Na_5Y_9F_{32}$:1 mol%Dy^{3+}/0.8 mol%Sm^{3+}	15.9	[67]

Table 3. A comparison of the PLQY values for $CaTiO_3$:4Dy^{3+}, $CaTiO_3$:4Dy^{3+}/2Ho^{3+} and $CaTiO_3$:3Ho^{3+} phosphors with the PLQY of other Dy^{3+} doped/co-doped phosphors.

The energy transfer efficiency is found to be maximum 67.76% and 69.39% for $CaTiO_3:4Dy^{3+}/3Ho^{3+}$ and $CaTiO_3:3Ho^{3+}/5Dy^{3+}$ phosphors, respectively. The CIE color coordinates and the correlated color temperature (CCT) of the phosphors have been calculated, which show color tunability from whitish to green via greenish yellow color. The lifetime of $^4F_{9/2}$ level of Dy^{3+} and $^5S_2$ level of Ho^{3+} ions are decrease in presence of Ho^{3+} and Dy^{3+} ions, respectively. This is due to energy transfer from Dy^{3+} to Ho^{3+} ions and vice versa. Temperature dependent photoluminescence spectra measurement has been carried out to know the thermal stability of phosphor materials for various applications. The temperature dependent photoluminescence spectra of $CaTiO_3:4Dy^{3+}/2Ho^{3+}$ phosphor shows high thermal stability (at 423 K is 82% of initial temperature 303 K) with activation energy 0.17 eV. We have also carried out the photoluminescence quantum yield (PLQY) measurements and it value in different cases are found to be 35% for $CaTiO_3:3Ho^{3+}$, 30% for $CaTiO_3:4Dy^{3+}$ and 33% for $CaTiO_3:4Dy^{3+}/2Ho^{3+}$ phosphors. Hence, Dy^{3+} and Ho^{3+} singly doped and Dy^{3+}/Ho^{3+} co-doped $CaTiO_3$ phosphor materials can be used in field of single matrix perovskite color tunable phosphors which may be suitable for multicolor display devices, near UV chip excited LED/WLED's for the solid state lighting applications and photodynamic therapy for cancer treatment.

Experimental section
Synthesis of materials
The phosphor samples were prepared by solid state reaction method. The starting chemicals were calcium carbonate ($CaCO_3$, 99.9%), titanium dioxide (TiO_2, 99.9%), dysprosium oxide (Dy_2O_3, 99.9%) and holmium oxide (Ho_2O_3, 99.9%). We prepared a series of samples of xDy^{3+} (x = 3.0, 4.0 & 5.0 mol %) and of yHo^{3+} (where y = 1.0, 3.0 & 5.0 mol %) doped $CaTiO_3$ phosphors to get the particular concentration of Dy^{3+} and Ho^{3+} ions, respectively for optimum PL emission. At the next step mixed samples of $CaTiO_3:xDy^{3+}:yHo^{3+}$ were synthesized to study the energy transfer and color tunability. For this we fixed the concentration of Dy^{3+} at 4 mol % (the concentration at which the emission intensity of Dy^{3+} was optimum) and varied the concentration of Ho^{3+} in $CaTiO_3:4Dy^{3+}/yHo^{3+}$ (where y = 0.5, 1.0, 1.5, 2.0 & 3.0 mol %) phosphors and also by fixing the concentration of Ho^{3+} at 3 mol % and varying the concentration of Dy^{3+} in $CaTiO_3:3Ho^{3+}/xDy^{3+}$ (where x = 1.0, 3.0 & 5.0 mol %) phosphors.

The pure chemicals were weighed carefully and mixed in an agate mortar using acetone as mixing medium for one hour. The samples were heated at 1473 K for 4 h in a programmable electrical furnace in air environment. The heated samples were cooled and crushed further to get fine powder. These powder samples were used for various characterizations.

Instrumentations
The crystallization and phase detection of phosphors were made by XRD measurements using CuK_α radiation ($\lambda = 0.15406$ nm) with MiniFlex600 (Rigaku, Japan). The morphology of phosphors were studied using FE-SEM with the help of Zeiss, Evo 18 Research system. The energy dispersive X-ray spectroscopic (EDX) measurements were carried out to verify the elements present in the phosphor materials. The Fourier transform infrared (FTIR) measurements were carried out to know the vibrational groups present in phosphor samples using PerkinElmer I-Frontier system in the 400–3000 cm^{-1} region. The photoluminescence excitation and emission spectra of the materials were monitored by using Fluorolog-3 spectrophotometer with 450W Xenon lamp as source (Horiba Jobin Yvon). We have also measured the lifetime of $^4F_{9/2}$ level of Dy^{3+} ion and $^5S_2$ level of Ho^{3+} ion in absence and presence of Ho^{3+} and Dy^{3+} ion, respectively using 25W pulsed xenon lamp attached with the same unit (Fluorolog-3 spectrophotometer). The absolute PLQY measurement was done with the help of Horiba PTI QuantaMaster-400 fluorescence spectrometer equipped with an integrating sphere.

Data availability
The datasets used and/or analysed during the current study are available from the corresponding author on request.

References
1. Singh, D. K. & Manam, J. Investigation of structural, spectral and photometric properties of $CaTiO_3:Dy^{3+}$ nanophosphors for the lighting applications. *Electron. Mater. Lett.* **13**, 292–301 (2017).
2. Singh, P., Yadav, R. S. & Rai, S. B. Enhanced photoluminescence in a Eu^{3+} doped $CaTiO_3$ perovskite phosphor via incorporation of alkali ions for white LEDs. *J. Phy. Chem. Solid.* **151**, 109916 (2021).
3. Singh, P., Yadav, R. S., Singh, P. & Rai, S. B. Upconversion and downshifting emissions of $Ho^{3+}-Yb^{3+}$ co-doped $ATiO_3$ perovskite phosphors with temperature sensing properties in $Ho^{3+}-Yb^{3+}$ codoped $BaTiO_3$ phosphor. *J. Alloys Compds.* **855**, 157452 (2021).
4. Dwivedi, A., Srivastava, M., Srivastava, A., Upadhyay, C. & Srivastava, S. K. Tunable photoluminescence and energy transfer of Eu^{3+}, Ho^{3+}-doped $Ca_{0.05}Y_{1.93-x}O_2$ nanophosphors for warm white LEDs applications. *Sci. Rep.* **12**, 5824 (2022).
5. Rao, R. P. & Devine, D. J. RE-activated lanthanide phosphate phosphors for PDP applications. *J. Lumin.* **87–89**, 1260–1263 (2000).
6. Xiong, F. B. *et al.* A novel white-light emission phosphor Dy^{3+}-doped $CaLaB_4O_{13}$ under UV Excitation. *Opt. Laser Technol.* **106**, 29–33 (2018).
7. de Leeuw, D. M., Mutsaers, C. A. H. A., Mulder, H. & Klaassen, D. B. M. Blue emitting phosphors for projection cathode ray tubes: (La, Y)OBr: Ce and (La, Gd)OBr:Ce. *J. Electrochem. Soc.* **135**, 1009 (1988).
8. Yadav, R. S., Dhoble, S. J. & Rai, S. B. Enhanced photoluminescence in Tm^{3+}, Yb^{3+}, Mg^{2+} tridoped $ZnWO_4$ phosphor: Three photon upconversion, laser induced optical heating and temperature sensing. *Sens. Actuators B Chem.* **273**, 1425–1434 (2018).
9. Wu, F. *et al.* Near-infrared emissive lanthanide hybridized carbon quantum dots for bioimaging applications. *J. Mater. Chem. B* **4**, 6366 (2016).
10. Johnson, L. F. & Guggenheim, H. Infrared-pumped visible laser. *Appl. Phys. Lett.* **19**, 44–47 (1971).

11. Van Der Ende, B. M., Aarts, L. & Meijerink, A. Lanthanide ions as spectral converters for solar cells. *Phys. Chem. Chem. Phys.* **11**, 11081–11095 (2009).
12. Liu, P., Wang, F. & Yang, B. Upconversion/downconversion luminescence of color-tunable Gd_2O_3:Er^{3+} phosphors under ultraviolet to near-infrared excitation. *Solid State Sci.* **102**, 106165 (2020).
13. Kaczmarek, A. M., Ndagsi, D. & Deun, R. V. Dopant and excitation wavelength dependent color tunability in Dy^{3+}:YVO_4 and Dy^{3+}/Eu^{3+}:YVO_4 microparticles towards white light emission. *Dalton Trans.* **45**, 16231–16239 (2016).
14. Tang, W. & Zhang, Z. Realization of color tuning via solid-solution and energy transfer in $Ca_{3-x}Sr_x(PO_4)_2$:Eu^{2+}, Mn^{2+} phosphors. *J. Mater. Chem. C* **3**, 5339–5346 (2015).
15. Chen, X., Xia, Z., Yi, M., Wu, X. & Xin, H. Rare-earth free self-activated and rare-earth activated $Ca_2NaZn_2V_3O_{12}$ vanadate phosphors and their color-tunable luminescence properties. *J. Phys. Chem. Solids.* **74**, 1439–1443 (2013).
16. Lohia, N. *et al.* Novel multi-wavelength excitable single-component phosphor system for application in white-LEDs. *Ceram. Int.* **46**, 4079–4085 (2020).
17. Zhang, X. *et al.* Luminescence and energy transfer of color-Tunable$Y_2Mg_2Al_2Si_2O_{12}$:Eu^{2+}, Ce^{3+}phosphors. *Inorg. Chem.* **60**, 5908–5916 (2021).
18. Hussain, S. K. *et al.* Energy transfer mechanism and tunable emissions from $K_3La(VO_4)_2$:Dy^{3+}/Eu^{3+} phosphors and soft-PDMS-based composite films for multifunctional applications. *J. Alloys. Comp.* **805**, 1271–1281 (2019).
19. Amador, E. *et al.* A new pyridinium-substituted tetraphenylethylene aggregation induced emission composites for rare-earth free white light displays. *Mater. Today. Phys.* **33**, 101036 (2023).
20. Qu, M., Zhang, X., Mi, X., Liu, Q. & Bai, Z. Novel color tunable garnet phosphor of Tb^{3+} and Eu^{3+} co-doped $Ca_2YZr_2Al_3O_{12}$ with high thermal stability via energy transfer. *J. Alloys. Comp.* **828**, 154398 (2020).
21. Li, K. & Deun, R. V. Color tuning from greenish-yellow to orange-red in thermal stable $KBaY(MoO_4)_3$:Dy^{3+}/Eu^{3+} phosphors via energy transfer for UV w-LEDs. *ACS Appl. Electron. Mater.* **2**(6), 1735–1744 (2020).
22. Rai, E., Roy, A., Rai, A., Fulari, V. J. & Rai, S. B. Structural and luminescent properties and energy transfer from Tb^{3+} to Eu^{3+} in $LaVO_4$:xTb^{3+}/yEu^{3+} phosphors. *J. Alloys Compds.* **937**, 168395 (2023).
23. Ratnam, B. V., Jayasimhadri, M., Kiwan, J., Sueb, L. H. & Y, S-S., Jeong, J-H. White light emission from $NaCaPO_4$: Dy^{3+} phosphor for ultraviolet-based white light-emitting diodes. *J. Am. Ceram. Soc.* **93**, 3857–3861 (2010).
24. Liu, Q. *et al.* White light emitting luminescent material $Ba_3Y(PO_4)_3$:Dy^{3+}. *Ceram. Int.* **40**, 10125–10129 (2014).
25. Kuang, J., Liu, Y. & Zhang, J. White-light-emitting long-lasting phosphorescence in Dy^{3+}-doped $SrSiO_3$. *J. Solid State Chem.* **179**, 266–269 (2006).
26. Singh, V., Dabre, K. V. & Lakshminarayana, G. Green emitting holmium (Ho) doped yttriumoxide (Y_2O_3) phosphor for solid state lighting. *Optik* **206**, 164339 (2020).
27. Singh, V. *et al.* Optical properties of $Sr_2La_8(SiO_4)_6O_2$ doped with Ho^{3+} phosphor. *Optik* **242**, 167268 (2021).
28. Zou, X. *et al.* X-ray-induced nanoparticle-based photodynamic therapy of cancer. *Nanomedicine* **9**(15), 2339–2351 (2014).
29. Liu, Y., Chen, W., Wang, S. & Joly, A. G. Investigation of water-soluble x-ray luminescence nanoparticles for photodynamic activation. *Appl. Phys. Lett.* **92**(4), 043901 (2008).
30. Liu, Y. *et al.* X-ray luminescence of LaF_3:Tb^{3+} and LaF_3:Ce^{3+}, Tb^{3+} water-soluble nanoparticles. *J. Appl. Phys.* **103**(6), 063105 (2008).
31. Kaur, S., Rao, A. S. & Jayasimhadri, M. Color tunability and energy transfer studies of Dy^{3+}/Eu^{3+} co-doped calcium aluminozincate phosphor for lighting applications. *Mater. Res. Bull.* **116**, 79–88 (2019).
32. Guan, H., Liu, G., Wang, J., Dong, X. & Yu, W. Tunable luminescence and energy transfer properties of $NaGdF_4$:Dy^{3+} Eu^{3+} nanophosphors. *New J. Chem.* **38**, 4901 (2014).
33. Fu, Y. *et al.* Electronic structure, energy transfer mechanism and thermal quenching behavior of $K_3YB_6O_{12}$:Dy^{3+}, Eu^{3+} phosphor. *Opt. Mater.* **99**, 109519 (2020).
34. Zhang, X. *et al.* Energy transfer from Bi^{3+} to Ho^{3+} triggers brilliant single green light emission in $LaNbTiO_6$:Ho^{3+}, Bi^{3+} phosphors. *RSC Adv.* **4**, 13680–13686 (2014).
35. Guan, H., Lib, Y. & Liu, G. A Novel Green emitting $NaGdF_4$: Dy^{3+}, Ho^{3+} phosphor with tunable photoluminescence. *New J. Chem.* **44**, 16211–16217 (2020).
36. Singh, P., Mishra, H., Pandey, P. C. & Rai, S. B. Structure, photoluminesence properties and energy transfer phenomenon in Sm^{3+}/Eu^{3+} co-doped $CaTiO_3$ phosphors. *New J. Chem.* **47**, 1460–1471 (2023).
37. Chauhan, V. *et al.* Effect of Zn^{2+} co-doping on the luminescence of Sm^{3+} doped $SrMoO_4$ phosphor. *J. Lumin.* **248**, 118994 (2022).
38. Monika., Yadav, R. S., Bahadura, A. & Rai, S. B. Multicolor tunable bright photoluminescence in Ca^{2+}/Mg^{2+} modified Eu^{3+} doped $ZnGa2O_4$ phosphors under UV excitation for solid state lighting applications. *RSC Adv.* **13**, 20164 (2023).
39. Dahiya, M., Siwach, A., Dalal, M. & Kumar, D. Study of structural and luminescent characteristics of novel color tunable blue-green Tb^{3+}-doped $Na_3Y(PO_4)_2$ nanoparticles for NUV-based WLEDs. *J. Mater. Sci. Mater. Elect.* **32**, 4166–4176 (2021).
40. Damodaraiah, S., Prasad, V. R. & Ratnakaram, Y. C. Structural and luminescence properties of Sm^{3+}-doped bismuth phosphate glass for orange-red photonic applications. *Luminescence* **33**, 594–603 (2018).
41. Liu, J., Tang, Q., Liu, Z., Zhang, W. & Qiu, K. Luminescence enhancement of $(Ca_{1-x}Mx)TiO_3$:Dy^{3+} phosphors through partial M (Mg^{2+}/Zn^{2+}) substitution for white-light-emitting diodes. *Ceram. Inter.* **44**, 14774–14780 (2018).
42. Dutta, S., Som, S. & Sharma, S. K. Excitation spectra and luminescence decay analysis of K^+ compensated Dy^{3+} doped $CaMoO_4$ phosphors. *RSC Adv.* **5**, 7380–7387 (2015).
43. Kolesnikov, I. E. *et al.* Structural, luminescence and thermometric properties of nanocrystalline YVO_4:Dy^{3+} temperature and concentration series. *Sci. Rep.* **9**, 2043 (2019).
44. Zhang, Y. *et al.* A new single-phase white-light emitting $CaWO_4$:Dy^{3+} phosphor: Synthesis, luminescence and energy transfer. *RSC Adv.* **5**, 62527–62533 (2015).
45. Lü, Y. *et al.* Synthesis and luminescent properties of $GdNbO_4$:RE^{3+} (RE = Tm, Dy) nanocrystalline phosphors via the sol-gel process. *J. Phys. Chem. C* **117**, 21972–21980 (2013).
46. Kumar, A., Couto, M. H. M., Tiwari, S. P., Kumar, K. & Esteves da Silva, J. C. G. Effect of pH of precursor on up/downconversion and cathodoluminescence of Gd_2O_3:Ho^{3+}/Yb^{3+} phosphor and magneto-optic studies. *Chem. Select.* **3**, 10566–10573 (2018).
47. Kumar, A. *et al.* Improvement in upconversion/downshifting luminescence of Gd_2O_3:Ho^{3+}/Yb^{3+} phosphor through Ca^{2+}/Zn^{2+} incorporation and optical thermometry studies. *Mater. Res. Bull.* **112**, 28–37 (2019).
48. Ren, Q. *et al.* Luminescence characteristics of a novel Tm/Eu co-doped polychromatic tunable phosphor. *J. Solid State Chem.* **294**, 121869 (2021).
49. Hossu, M., Liu, Z., Yao, M., Ma, L. & Chen, W. X-ray luminescence of CdTe quantum dots in LaF_3:Ce/CdTe nanocomposites. *Appl. Phys. Lett.* **100**, 013109 (2012).
50. Yao, M. *et al.* Luminescence enhancement of CdTe nanostructures in LaF_3:Ce/CdTe nanocomposites. *Appl. Phys.* **108**, 103104 (2010).
51. Li, K. & Deun, R. V. Photoluminescence and energy transfer properties of a novel molybdate $KBaY(MoO_4)_3$:Ln^{3+} (Ln^{3+} = Tb^{3+} Eu^{3+} Sm^{3+} Tb^{3+}/Eu^{3+} Tb^{3+}/Sm^{3+}) as a multi-color emitting phosphor for UV w-LEDs. *Dalton Trans.* **47**, 6995–7004 (2018).
52. Meza-Rochaa, A. N., Bordignonb, S., Speghinib, A., Lozada-Moralesd, R. & Caldiño, U. Zinc phosphate glasses activated with Dy^{3+}/Eu^{3+}/Sm^{3+} and Tb^{3+}/Eu^{3+}/Sm^{3+} for reddish orange and yellowish white phosphor applications. *J. Lumin.* **203**, 74–82 (2018).
53. Chen, W., Aguekian, V. F., Vassiliev, N., Serov, A. Y. & Filosofov, N. G. New observations on the luminescence decay lifetime of Mn^{2+} in ZnS:Mn^{2+} nanoparticles. *J. Chem. Phys.* **123**(12), 124707 (2005).

54. Liu, X. *et al.* Controllable synthesis of uniform CaMoO$_4$:Eu^{3+}, M$^+$ (M = Li, Na, K) microspheres and optimum luminescence properties. *RSC Adv.* **5**, 9441–9454 (2015).
55. Chen, W., Joly, A. G. & McCready, D. E. Upconversion luminescence from CdSe nanoparticles. *J. Chem. Phys.* **122**(22), 224708 (2005).
56. Dwivedi, A., Singh, A. K. & Rai, S. B. Down-shifting and upconversion photoluminescence in Ho^{3+}/Yb^{3+} codoped GdNbO$_4$: Effect of the Bi^{3+} ion and the magnetic field. *Dalton Trans.* **43**, 15906–15914 (2014).
57. Mahata, M. K., Koppe, T., Kumar, K., Hofsäss, H. & Vetter, U. Upconversion photoluminescence of Ho^{3+}-Yb^{3+} doped barium titanate nanocrystallites: Optical tools for structural phase detection and temperature probing. *Sci. Rep.* **10**, 8775 (2020).
58. Tang, H. *et al.* Tunable emission in Dy^{3+}/Eu^{3+}-doped BaLu$_2$Si$_3$O$_{10}$ trisilicate structure for white light-emitting diode applications. *J. Alloys Compds.* **934**, 168068 (2023).
59. Zhao, J. *et al.* Single-phase white-emitting phosphors Ba$_3$Bi(PO$_4$)$_3$:Dy^{3+}, Eu^{3+} with tunable correlated color temperature and high thermal stability towards light emitting applications. *J. Mater. Sci. Mater. Electron.* **32**, 28077–28087 (2021).
60. Naresh, V. & Lee, N. Energy transfer dynamics in thermally stable single-phase LiMgBO$_3$:Tm^{3+}/Dy^{3+} phosphor for UV triggered white light-emitting devices. *Mater. Sci. Engin. B* **271**, 115306 (2021).
61. Fan, B., Zhao, W. & Han, L. Eu^{3+} co-doped Sr$_3$Gd(PO$_4$)$_3$:Dy^{3+} phosphors: Luminescence properties and color-tunable white-light emission for NUV-WLEDs. *Appl. Phys. A.* **126**, 1–10 (2020).
62. Su, L. *et al.* Structure and luminescent properties of new Dy^{3+}/Eu^{3+}/Sm^{3+}-activated InNbTiO$_6$ phosphors for white UV-LEDs. *Opt. Mater.* **98**, 109403 (2019).
63. Wei, Y. *et al.* Highly efficient blue emission and superior thermal stability of BaAl$_{12}$O$_{19}$:Eu^{2+} phosphors based on highly symmetric crystal structure. *Chem. Mater.* **30**, 2389–2399 (2018).
64. Wang, L., Xu, M., Zhaoa, H. & Jia, D. Luminescence, energy transfer and tunable color of Ce^{3+}, Dy^{3+}/Tb^{3+} doped BaZn$_2$(PO$_4$)$_2$ phosphors. *New J. Chem.* **40**, 3086–3093 (2016).
65. Jamalaiah, B. C. & Babu, Y. R. Near UV excited SrAl$_2$O$_4$:Dy^{3+} phosphors for white LED applications. *Mater. Chem. Phys.* **211**, 181–191 (2018).
66. Bedyal, A. K., Kunti, A. K., Kumar, V. & Swart, H. C. Effects of cationic substitution on the luminescence behavior of Dy^{3+} doped orthophosphate phosphor. *J. Alloys Compds.* **806**, 1127–1137 (2019).
67. Xu, F., Zhou, X., Xia, H., Song, H. & Chen, B. Highly thermally stable Dy^{3+}/Sm^{3+} co-doped Na$_5$Y$_9$F$_{32}$ single crystals for warm white LED. *J. Phys. Chem. Solid* **158**, 110240 (2021).

Acknowledgements

Author contributions

P.S. Methodology, conceptualization, data collection, visualization, validation, writing-original draft, writing review and; editing; H.M. review, editing and suggestion; S.B.R. Conceptualization, supervision, visualization, review and; editing.

Competing interests

The authors declare no competing interests.

Additional information

Correspondence and requests for materials should be addressed to S.B.R.

Reprints and permissions information is available at www.nature.com/reprints.

Publisher's note Springer Nature remains neutral with regard to jurisdictional claims in published maps and institutional affiliations.